PNC-TN9410 89-159

VALIDATION OF FILM DRYOUT MODEL IN A THREE-FLUID CODE FIDAS

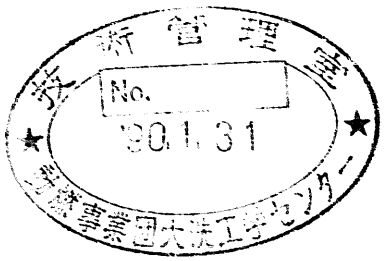

November 1 9 8 9

Power Reactor and Nuclear Fuel Development Corporation
O-arai Engineering Center

PNC-TN9410 89-159
November 1989

VALIDATION OF FILM DRYOUT MODEL IN A THREE-FLUID CODE FIDAS

Satoru Sugawara

ABSTRACT

Analytical prediction model of critical heat flux (CHF) has been developed on the basis of film dryout criterion due to droplets deposition and entrainment in annular mist flow. CHF in round tubes were analyzed by the Film Dryout Analysis Code in Subchannels, FIDAS, which is based on the three-fluid, three-field and newly developed film dryout model. Predictions by FIDAS were compared with the world-wide experimental data on CHF obtained in water and Freon for uniformly and non-uniformly heated tubes under vertical upward flow condition. Furthermore, CHF prediction capability of FIDAS was compared with those of other film dryout models for annular flow and Katto's CHF correlation. The predictions of FIDAS are in sufficient agreement with the experimental CHF data, and indicate better agreement than the other film dryout models and empirical correlation of Katto.

Reactor Engineering Section, Safety Engineering Division,
PNC-OEC

LIST OF TABLES

LIST OF FIGURES

Fig.10 Comparison between Predicted and Measured CHF (Effect of Pressure; data base are same as Fig.9)

Fig.11 Comparison between Predicted and Measured Effect of Diameter on CHF

Fig.12 Comparison between Predicted and Measured CHF in q_{cr} vs. x_{eq} Plane (Effect of Heated Length)

Fig.13 Comparison between Predicted and Measured Dryout Power with Various Type of Axial Power Distributions

AERE-R5076[22]
l_H= 3.658m
D = 12.57mm
Inlet peaked
◇ q_{max}/q_{min}=3.73
+ q_{max}/q_{min}=2.99
☆ q_{max}/q_{min}=1.91

□AEEW-R355[23]
l_H= 3.658m
D = 9.47mm
Cosine(APF=1.40)

○AERE-R356[16]
l_H= 3.658m
D = 10.82mm
Uniform

Fig.14 Comparison between Predicted and Measured CHF for Freon-12

Fig.15 Effect of $t_{F,cr}$ and m_B on CHF Prediction (data base are same as Fig.9)

Fig.16 Comparison between Present Analysis and Other Correlations (modified from Ref.[21])

○: Ref.[16], P=6.7-7.1MPa, D=10.8mm, l_H=0.43-3.05m
●: Ref.[3], P=7.0MPa, D=10.0mm, l_H=2.02-8.00m
X: Ref.[26], P=7.0MPa, D=10.0mm, l_H=2.0m

Fig.17 Examination of CHF Prediction Capability comparing with Katto's Correlation (#1: Dependence of CHF on Mass Velocity)

Fig.18 Examination of CHF Prediction Capability comparing with Katto's Correlation (#2: Dependence of CHF on Inlet Subcooling)

Fig.19 Examination of CHF Prediction Capability comparing with Katto's Correlation (#3: Dependence of CHF on Steam Quality)

Fig.20 Examination of CHF Prediction Capability comparing with Katto's Correlation (#4: Dependence of CHF on Pressure)

I. INTRODUCTION

Prediction of dryout occurrence is one of primary concern in water-cooled nuclear reactor design and safety evaluations. A number of empirical correlations on CHF have been developed from accumulated experimental data and widely applied to design and safety evaluations. However, a result of this situation is that the empirical correlations are restricted to ranges within experimental conditions.

One of the possible approaches in resolving this issue is phenomenological modeling to treat the dryout phenomenon on the basis of multi-fluid modeling coupled with the annular flow film dryout criterion. Actually, some attempts have been made recently to predict the dryout occurrence by the annular flow modeling coupled with a film dryout criterion.[1][2][3][4] However, at present, attained capabilities are insufficient for practical purposes because of incomplete modeling in droplet entrainment and deposition which play significant role in the analytical prediction of dryout.[5]

Therefore, in the previous study[6], the interfacial mass transfer models for droplet entrainment from roll waves and droplet deposition from gas core onto liquid film have been developed. Film Dryout Analysis Code in Subchannels (FIDAS) has been also developed on the basis of the three-fluid model for simulating the interfacial transfer phenomena between phases and for predicting the dryout occurrence in channels and in rod bundles.[7][8][9] Indeed, validation study of the developed interfacial mass transfer models for droplet entrainment and deposition coupled with FIDAS code were carried out by focusing the hydrodynamic equilibrium flow rates of entrained droplets and liquid film for adiabatic annular mist flow.[6] The validation study indicates that the developed models have good capabilities in predicting the hydrodynamic equilibrium flow rates of droplets and liquid film and their dependence on the steam quality, mass flux, tube diameter and pressure in adiabatic annular-mist two phase flow, through comparisons with the experiments by Hewitt et al.[10], Keeys et al.[11], Yanai[12] and Wurtz[3].

Furthermore, in the present study, physical models for mass transfer phenomenon due to vaporization in diabatic flow are newly derived on the suppression of droplet deposition and on the

maximum film thickness limitation by Helmholtz instability due to nucleate boiling in the liquid film. Validation study of developed models on CHF prediction is also presented by comparing with a large number of experimental CHF data for uniformly and non-uniformly heated round tubes in vertical upward flow using water and Freon. In addition, CHF prediction capability of FIDAS code incorporated with the derived models is compared with those of well-known Katto's CHF correlation[18] and other film dryout models presented by Whalley[1], Wurtz[3] and Levy[4] to demonstrate the performance of developed models with FIDAS.

II. FORMULATION AND CALCULATIONAL FEATURE OF THE FIDAS CODE

FIDAS provides a three-fluid, three-field representation of two-phase flow in a channel or rod bundles. The three fields are specified by continuous liquid film, continuous vapor and entrained droplets suspended in vapor. In order to predict the dryout occurrence on heated surface, the code provides the capability to simulate flow regime evolution in a channel as shown in Fig.1; i.e. single-phase liquid flow at the entrance, bubbly/slug flow formulation by evaporation, transition to a liquid-vapor-droplet annular flow, a further transition to vapor-droplet mist flow due to liquid film disappearance on the heated surface, and superheated single-phase vapor flow formulation due to complete evaporation of all droplets. In this evolution process, the onset of dryout is defined as the disappearance of liquid film adhering on the heated surface.

The computational scheme of the code is constructed on the basis of a semi-implicit method. A staggered mesh is used, and the time step is adjusted according to velocity limits expressed by the Courant number. The specifications for boundary conditions are the inlet velocity (or mass flux), inlet temperature (or enthalpy), heat flux to the wall, and the outlet pressure. The conservation equations are described in Ref.[7].

III. PHYSICAL MODELS AND CONSTITUTIVE EQUATIONS

1. Interfacial Mass Transfer Model due to Entrainment and Deposition

As shown in Fig.2, the local film flow rate is calculated as a function of distance along the channel from the following mass

balance equation:

$$\frac{dW_F}{dz} = \pi D \left[(m_D - m_B) - m_E - \frac{q_w}{H_{lg}} \right] \quad , \tag{1}$$

where W_F is the mass flow rate of liquid film, z the distance along the channel, D the tube diameter, m_D the rate of droplet deposition per unit area of the tube wall, m_E the rate of entrainment per unit area, m_B, which is proposed in the present study, the suppression rate of droplet deposition by vaporization per unit area, q_w the heat flux, and H_{lg} the latent heat of vaporization.

The deposition rate, m_D is calculated at each position from the relationship,

$$m_D = k_D C \quad , \tag{2}$$

where k_D is a deposition coefficient and C is the concentration of droplets in the vapor core.

The deposition coefficient, k_D is estimated from the following correlation derived by Sugawara[6].

$$\frac{k_D}{u_G} = 9.0 \times 10^{-3} \left(\frac{C}{\rho_G}\right)^{-0.5} Re_G^{-0.2} Sc^{-2/3} \tag{3}$$

with,

$$C = \frac{W_E}{\frac{W_G}{\rho_G}\frac{u_E}{u_G} + \frac{W_E}{\rho_E}} \tag{4}$$

In this expression, Schmidt number is calculated using the Lewis' relation, i.e. Le≒ 1.

The entrainment rate, m_E is estimated from the following correlation developed by Sugawara[6]:

$$m_E = 1.07 S_R \tag{5}$$

$$S_R = \left(\frac{\tau_{FG} \Delta h_{eq}}{\sigma}\right)\left(\frac{u_G \mu_E}{\sigma}\right)\left(\frac{\rho_E}{\rho_G}\right)^{0.4} \tag{6}$$

with,

$$\Delta h_{eq} = k_S \qquad (Re_G \geq 1\times10^5) \ , \quad (7a)$$

$$\Delta h_{eq} = k_S \ (2.13 \log_{10}(Re_G) - 9.68) \qquad (Re_G < 1\times10^5) \ , \quad (7b)$$

$$(\ \Delta h_{eq} > 0.0 \ )$$

$$k_S = 0.57 \ t_F + 21.73\times10^3 \ t_F^2 - 38.8\times10^6 \ t_F^3 + 55.68\times10^9 \ t_F^4 \ , \quad (8)$$

where, τ_{FG} is the interfacial shear stress between liquid film and gas core, Δh_{eq} the equivalent height of roll waves, t_F the mean film thickness, σ the surface tension and k_S the sand roughness of roll waves presented by Wurtz[3]. Detailed derivation, validation and applicable range of these correlations for entrainment and deposition are described in Ref.[6].

2. Suppression of Droplet Deposition due to Vaporization

An effect of vaporization of liquid film on the interfacial mass transfer should be additionally considered in diabatic condition. It is postulated in diabatic flow that bubble formation in the liquid film and bubble burst at the film surface cause an increment of the entrainment rate and that perpendicular vapor flow by evaporation of the liquid film diminishes the droplet deposition rate. Thus, the interactions between the heat flux and the droplet exchange process have been studied in several papers[3][20]. According to these studies, however, enhancement of the entrainment rate in former case is supposed to be negligible for the moderate heat flux ($q<2MW/m^2$). Hence, under the moderate heat flux ($q<2MW/m^2$) condition, the effect of vaporization on the interfacial mass transfer could resolve itself into the suppression effect on droplet deposition as shown in Fig.3.

Assuming $D_1 \fallingdotseq D$, the radial velocity of the steam at the film surface is given by:

$$u_B = \frac{q_w}{H_{lg} \ \rho_G} \ . \quad (9)$$

This velocity is considered to decrease significantly with distance from the wall due to the turbulent diffusion of vapor

core. At large film thickness, where the height of roll waves is large, the influence of the perpendicular gas stream on the deposition rate is assumed to be negligible, because droplets are captured by roll waves at relatively large distance from the wall. On the contrary, at small film thickness, where the film is relatively smooth, it is assumed that the radial gas stream significantly affects the droplet deposition. Therefore, assuming u_B decreases exponentially with the distance from the heated wall, the suppression rate of droplet deposition by vaporization, m_B could be calculated as follows:

$$m_B(y=t_F) = u_B \exp(-t_F/t_{F,o})\, C$$

$$= \left(\frac{q_w}{H_{lg}\,\rho_G}\right) \exp(-t_F/t_{F,o})\, C \quad , \qquad (10)$$

with $\quad m_B \leqq m_D \quad ,$

where $t_{F,o}$ is the reference film thickness. From a consideration on the universal velocity profile, $t_{F,o}$ is presumed to be correlated with the thickness of laminar sublayer or buffer layer. Hence, $t_{F,o}$ can be given by:

$$t_{F,o} = c_{F,o}\, y(y^+=30)$$

$$= c_{F,o} \left(\frac{30\,\nu_F}{\sqrt{\tau_{wF}/\rho_F}}\right) \quad , \qquad (11)$$

where $c_{F,o}$ is an experimentally determined parameter, y^+ is the non-dimensional film thickness, and $y^+=30$ is the transition point from the buffer layer to turbulent core in the universal velocity profile.

From comparisons with available CHF data, a recommended value of $c_{F,o}$ is estimated as follows:

$$c_{F,o} = 158.7 \left(\frac{\mu_G}{\mu_L}\right)^{2.66} \quad , \qquad (12)$$

as indicated in Fig.4. A typical value of $c_{F,o}$ is 2.5 (i.e. $y^+=75$) at 7 MPa. Consequently, the suppression term of droplet deposition is expressed as a following correlation:

$$m_B(y=t_F) = u_B \exp(-t_F/t_{F,o})\ C$$

$$= \left(\frac{q_w}{H_{lg}\ \rho_G}\right) \exp\left[-\frac{t_F \sqrt{\tau_{wF}/\rho_F}}{158.7(\mu_G/\mu_L)^{2.88}\ 30\nu_F}\right] C\ ,$$

with $m_B \leqq m_D$. (13)

3. Maximum Film Thickness Limitation due to Vaporization

According to Haramura and Katto[13], the maximum film thickness $t_{F,cr}$ is restricted by Helmholtz instability under higher heat flux condition due to nucleate boiling in the liquid film as shown in Fig.5. From the critical wave length due to Helmholtz instability, they reported that $t_{F,cr}$ could be estimated as follows by assuming $(\rho_G/\rho_F)<<1$ and forced convective effect of film flow on this instability is negligible:

$$t_{F,cr} \propto \frac{\pi\ \sigma}{2} \left(\frac{\rho_F + \rho_G}{\rho_F\ \rho_G}\right) \left(\frac{\rho_G\ H_{lg}}{q_w}\right)^2 \left(\frac{A_G}{A_w}\right)^2\ , \qquad (14)$$

where A_G is the sum of the projected areas of vapor chimney in the liquid film per unit area, A_w is the unit area of heater surface, and $(A_G/A_w)^2$ is an experimentally determined parameter. Therefore, in the present study, a suitable value of $(A_G/A_w)^2$ is determined by comparing with available CHF data and by taking account of the effects of (ρ_G/ρ_F) and film flow on $(A_G/A_w)^2$ which have been neglected in derivation of Eq.(14). Figures 6(a) and 6(b) show obtained value of $(A_G/A_w)^2$ at P=7MPa and G=1000kg/m^{2}s. Consequently, the following correlation was obtained on the value of $(A_G/A_w)^2$:

$$\left(\frac{A_G}{A_w}\right)^2 = f_P \times f_G\ , \qquad (15a)$$

$$f_P = 9.832\times10^{-4} \left(\frac{\rho_G}{\rho_F}\right)^{-0.230} \quad (\rho_G/\rho_F \leqq 10^{-2}) \qquad (15b)$$

$$\log_{10}(f_P) = -0.746\ [\log_{10}\left(\frac{\rho_G}{\rho_F}\right) + 2.130]^2 - 2.535 \quad (\rho_G/\rho_F > 10^{-2}) \qquad (15c)$$

$$f_G = \mathrm{MIN.}[(G/G_o)^{1.34},\ (G/G_o)^{-0.80}] \quad (15d)$$

where G_o is a reference mass velocity set at 1000kg/m²s. Experimental data used in determination of Eq.(15a), (15b), (15c) and (15d) ranges in (ρ_G/ρ_F) of 6×10^{-4} to 1.3×10^{-1} and G of 550 to 4000kg/m²s. Equations (12), (13), (14) and (15) are improved from the view point of application to Freon from the previous study[7].

4. Flow Regime Transition to Annular Flow

As mentioned previously, it is necessary to give a criterion of the flow regime transition to annular flow, that is, the vapor volumetric fraction at the transition point, $\alpha_{G,tr}$. Fortunately, predicted CHF by film dryout model is insensitive to the transition criterion to annular flow similar to previous study by Whalley[1]. Hence, annular flow is assumed to start when α_G reaches the value obtained from the following equation formulated from the slug/annular transition boundary in the well-known Baker flow regime diagram[29].

$$\alpha_{G,tr} = \left(\frac{P+0.9}{P_o}\right) \exp\left(-\frac{G}{G_o}\right) + \left(\frac{3.1-P}{P_o}\right) \quad \text{(for water)} \quad (16a)$$

$$\alpha_{G,tr} = \left(\frac{P+2.1}{P_o}\right) \exp\left(-\frac{G}{G_o}\right) + \left(\frac{2.9-P}{P_o}\right) \quad \text{(for Freon)} \quad (16b)$$

where P_o and G_o are reference pressure and mass velocity set at 4.0MPa and 720kg/m²·s respectively.

5. Initial Entrainment Fraction

The initial entrainment fraction at the onset of annular flow, $\alpha_{E,ini}$ is also an important factor in the film dryout analysis, particularly in the shorter boiling length and high heat flux situation. In general, the relation between initial film thickness and $\alpha_{E,ini}$ at the onset of annular flow can be expressed as follows:

$$t_{F,ini} = \frac{(1 - \sqrt{(\alpha_{E,ini} + \alpha_{G,ini})})\ D}{2} \quad (17)$$

If the value of $t_{F,ini}$ obtained by Eq.(17) is greater than $t_{F,cr}$ obtained by Eqs. (14) and (15), $t_{F,cr}$ is used as a value of $t_{F,ini}$.

The initial condition of the calculation is given from the results for bubbly/slug flow regime in which u_G, u_L and α_G are estimated by the drift flux model of Zuber[27], and pressure drop is calculated by a following equation[28].

$$\phi_{lo}^2 = (1 - \alpha_G)^{-m} \text{ , with } m=1.75. \qquad (18)$$

6. Other Constitutive Equations and Comments

The following constitutive equations are provided in the code in addition to the above mentioned models and equations.

(a) Wall shear stress, between wall and liquid film in the pre-dryout region, and between wall and vapor in the post-dryout region.
(b) Vapor-liquid and vapor-droplet interfacial drag forces.
(c) Droplet size.

These constitutive equations are shown in Table 1. The interfacial shear stress between liquid film and vapor is estimated by the well-known Wallis correlation; the wall shear stress and drag force of droplet are given by conventional single phase correlations. Furthermore, the average droplet diameter is determined from the critical Weber number.

A step-by-step calculation along heated channel is carried out starting from the initiation of annular flow to the outlet with the given boundary condition. The CHF and dryout location can be predicted with the criteria that the film flow rate less than or equal to the critical film fraction ($\alpha_{F,cr} \leqq 10^{-5}$). Indeed, the node length is set at short enough to eliminate a numerical error on dryout prediction.

IV. ANALYTICAL RESULTS

1. Assessment of the Interfacial Exchange Model in Diabatic Flow

Measurements of liquid film and entrained droplet flow rates along heated channel in steam-water two-phase flow were carried out under the condition at which dryout just occurred at the test section outlet by Bennett et al.[14], Keeys et al.[15] and

Wurtz[3]. These experimental data were used to validate the interfacial exchange model of FIDAS. Typical comparison between analysis and experiment for the diabatic condition are indicated in Fig.7. As clearly seen in the figure, tracking capability of the prediction by FIDAS is significantly improved near the dryout position by the suppression model of droplet deposition introduced in the present study. In consequence,. analysis traces well the measured variation of flow rates of liquid film and entrainment along a heated channel at different mass velocity. In addition, measured dryout points are well predicted as the condition at which film flow reaches zero.

It is suggested from the figure that the developed interfacial exchange model with FIDAS is appropriate to simulate the behavior of annular mist flow in a heated channel.

2. CHF Prediction Capability for Uniformly Heated Round Tubes in Water

CHF data base used in the present study are those edited by Thompson-Macbeth[16] and those obtained by Bennett et al.[17] and Wurtz[3]. Selection of these data base were carried out to treat only CHF data in annular flow by using criteria which are $\alpha_{G,ex} > \alpha_{G,tr}$ and D≧ 3.0mm. In consequence, over 3,000 points of data are selected and cover the following wide range of parameters affecting CHF for uniformly heated tubes.

· Pressure	;	0.1 - 14	MPa
· Mass velocity	;	40 - 5300	kg/m²s
· Inlet subcooling	;	0 - 900	kJ/kg
· Steam quality	;	0.08 - 1.00	
· Heated length	;	0.15 - 8.0	m
· Inner diameter of tube	;	3.0 - 38.5	mm
· Boiling length/Inner diameter	;	13 - 770	

Measured CHF under above mentioned conditions ranges from 0.3 to 7.4 MW/m². From these data base, approximately 1200 points of CHF data are chosen by random sampling and used for validation analysis.

In general, the CHF for uniformly heated round tubes, in which the fluid fed to the channel is subcooled and flows upward,

is affected by five major independent variables; the inlet flow rate, the inlet temperature, the system pressure, the tube internal diameter, and the heated length. Therefore, the CHF prediction capability of the FIDAS are examined through comparisons with the dependence of measured CHF on these variables.

Typical comparisons between the predicted CHF by FIDAS and the experimental data are shown in Figs. 8 to 12. As can be seen in these figures, there are satisfactory agreements between the predicted CHF and experimental data. Additional comparisons are also shown in Figs.17 and 18 with over 1,200 points of the CHF data base obtained in uniformly heated vertical round tubes. It is recognized in these figures that the dependence of CHF on the major independent variables affecting the CHF can be well tracked by FIDAS together with film dryout model developed in the present study.

3. CHF Prediction Capability for Non-Uniformly Heated Round Tubes in Water

Experimental data of Hewitt et al.[22] and Lee et al.[23] were used to validate the CHF prediction capability of FIDAS for non-uniformly heated round tubes in water. Axial heat flux distribution used in the experiment of Hewitt et al. are inlet peaked ones with three different peaking factor. On the contrary, Lee et al. uses a cosine type profile with peaking factor of 1.4. Typical comparisons of dryout power are indicated in Fig.13 in which experimental data for a uniformly heated tube are also shown as a reference. Prediction of FIDAS traces well the dependence of measured dryout power on the axial heat flux profile.

4. CHF Prediction Capability for Uniformly Heated Round Tubes in Freon

CHF prediction capability of FIDAS for round tubes in Freon were also examined comparing with the experiments of Stevens et al.[24] and Barnett et al.[25] in which axial heat flux distribution is uniform. Typical comparison between predicted CHF by FIDAS and experimental data is indicated in Fig.14 at different heated length and mass velocity. Measured CHF in Freon

can be well predicted by FIDAS as shown in Fig.14. This indicates that FIDAS coupled with developed film dryout model can be applicable for Freon.

V. DISCUSSION

1. Effects of Droplet Deposition Suppression and Maximum Film Thickness Limitation Models

The models of suppression of droplet deposition due to film vaporization and maximum film thickness limitation due to Helmholtz instability were derived and used in the present study. The effect of the suppression term of droplet deposition can be shown in Fig.7 for film flow prediction. It should be noted from this figure that the effect of droplet deposition suppression by vaporization is recognized to be significant near the dryout points, and that this produces improved prediction of dryout. Figure 15 also indicates effects of these models on CHF prediction. As is seen in the figure, prediction accuracy on CHF is improved by droplet suppression model in the region of high l_B/D ratio (e.g. $l_B/D>300$ in the present case), where CHF is comparatively low. This suggests that the CHF in this region is dominated by the droplet exchange phenomenon between liquid film and vapor core. On the other hand, prediction accuracy on CHF is improved by maximum film thickness limitation model in the range of low l_B/D ratio (e.g. $l_B/D<300$ in the present case), where CHF is relatively high. Thus, the film thickness t_F of annular flow in tubes should be assumed as $t_F=t_{F,cr}$ as shown in Eqs.(14) and (15) instead of t_F obtained by Eq.(17).

2. Comparison with Other Film Dryout Models and Empirical CHF Correlations

Recently, Katto[18][19] gave an excellent review concerning CHF data in round tubes under vertical upflow conditions, and presented a good empirical CHF correlation on the basis of the newly derived non-dimensional parameter. In addition, theoretical analysis of the CHF based on the annular mist flow film dryout model have been presented by Whalley et al.[1], Saito[2], Wurtz[3], and Levy et al.[4] Therefore, CHF prediction capability of FIDAS is compared with the empirical correlation of Katto and these film dryout models. The comparisons between

predicted and measured CHF are indicated in Fig.16 together with the calculational condition shown in Table 2. As is seen in Fig.16, it can be said that the FIDAS prediction gives the better agreement in comparison with other film dryout models and the empirical correlation of Katto. Thus, the FIDAS prediction agrees with the experimental data over the entire experimental range of steam quality due to introduction of the models on droplet deposition suppression and on the maximum film thickness limitation due to Helmholtz instability theorem. On the contrary, the other film dryout models significantly overestimate the CHF in the lower quality region, although these models trace the trend of experimental data in higher quality region.

Furthermore, Figs.17 to 23 show comparison of CHF prediction capability between FIDAS and Katto's CHF correlation for previous mentioned over 1,200 points of the CHF data base obtained in uniformly heated vertical round tubes. It is denoted from the figure that CHF prediction capability of the FIDAS is better than that of Katto's correlation under the whole range of experimental conditions described in Sec.IV.2.

Finally, Fig.24 shows the comparison of statistical deviation of (predicted CHF)/(measured CHF) between FIDAS prediction and Katto's correlation. In the FIDAS prediction, approximately 99% of experimental data lie within ± 30% error band with standard deviation σ =0.105, while experimental data lie within ± 40% error band with standard deviation σ =0.137 in the case of Katto's CHF correlation. Particularly, it should be noted that FIDAS prediction based on the film dryout model gives better agreement in higher steam quality and lower heat flux region than that of Katto's correlation which has been derived fundamentally from the CHF data for heaters cooled by a jet of saturated liquid.

3. Influence of Uncertainties

One of the important problems in this kind of analysis is how analyzed results are affected by uncertainties of analytical assumptions and constitutive equations. Therefore, sensitivity analyses were carried out to examine the influences of these uncertainty on analytical results. Three experimental CHF data shown in Table 3 are chosen as representatives for the present

sensitivity analysis from the view point to cover a wide range of steam quality. Results of sensitivity analysis are summarized in Table 4 as variations of the predicted CHF from the nominal value. As shown in Table 4, most of variations of predicted CHF by these uncertainties of ± 20% are less than ± 5%. This leads a conclusion that these influence signify little to the present analysis.

VI. CONCLUSIONS

An theoretical analysis model for predicting CHF has been developed on the basis of the film dryout criterion. A validation study of the FIDAS code, which is based on the three-fluid model, coupled with the developed model has been also performed by comparing with experimental data of film flow rate under diabatic condition, and of CHF for uniformly and non-uniformly heated round tubes in water and Freon.

The validation study indicates that FIDAS can successfully analyze these important phenomena in annular mist two-phase flow. Particularly, CHF for round tubes can be successfully predicted by FIDAS in whole range of experimental conditions for both of water and Freon. In addition, it is clearly demonstrated that CHF prediction capability of the FIDAS is better than those of other film dryout models and empirical CHF correlation of Katto, due to introduction of the developed models including the droplet deposition suppression and the maximum film thickness limitation.

Consequently, it is concluded that the FIDAS code and its models are appropriate for application to predict CHF.

ACKNOWLEDGMENT

The author would like to express his appreciation to Professor A.Inoue of Tokyo Institute of Technology for valuable discussion and comments. The author appreciates to Dr. K.Shiba for his support of this study. The author thanks Mr. H.Kato, Mr. K.Watanabe and Mr. K.Komatsuzaki for their vigorous assistance in the analytical calculations.

NOMENCLATURE

$\overline{A}$ = interfacial area per unit volume, 1/m
C = droplet concentration, kg/m³
CHF = critical heat flux, W/m²
D = diameter, m
f = friction factor, -
G = mass flux, kg/(m²·s)
H = specific enthalpy, J/kg
H_{lg} = latent heat, J/kg
Δh = wave height, m
K = drag coefficient, -
k_D = deposition coefficient, m/s
L_e = Lewis number (= Sc/Pr), -
l = length, m
m_D = deposition rate of droplets onto the liquid film, kg/(m²·s)
m_B = suppression rate of droplets deposition due to evaporation, kg/(m²·s)
m_E = entrainment rate of droplets from the liquid film by roll waves, kg/(m²·s)
P = pressure, MPa
Pr = Prandtl number, -
q = heat flux, W/m²
Re = Reynolds number, -
Sc = Schmidt number, -
Sh = Sherwood number, -
t_F = film thickness, m
u = axial velocity, m/s
W = mass flow rate, kg/s
We = Weber number, -
x = steam quality, -
y = distance from the wall, m
z = distance, m

Greek letters

α = volumetric fraction, -
μ = dynamic viscosity, NS/m²
ν = kinetic viscosity, m²/s
ρ = density, kg/m³
σ = surface tension, N/m

τ = shear stress, N/m^2

ϕ_{lo}^2 = two-phase multiplier of pressure drop, -

Subscripts

B = boiling
cr = critical
E = entrainment or energy
F = liquid film
G = steam (gas core)
g = gas phase
i = interface
ini = initial
l = liquid phase
tr = transition
W = heated wall

REFERENCES

[1] Whalley, P.B., The calculation of dryout in a rod bundle, Int. J. of Multiphase Flow, 3(1977), 501-515.

[2] Saito, T., Hughes, E.D. and Carbon, M.W., Multi-fluid modeling of annular two-phase flow, Nucl. Eng. & Design, 50(1978), 225-271.

[3] Wurtz, J., An experimental and theoretical investigation of annular steam-water flow in tubes and annuli at 30 to 90 bar, RISO Report No.372(1978).

[4] Levy, S., Healzer, J.M. and Abodollahian, D., Prediction of critical heat flux in vertical pipe flow, Nucl. Eng. & Design, 65(1981), 131-140.

[5] Owen, D.G. and Hewitt, G.F., A proposed entrainment correlation, AERE-R12279(1986).

[6] Sugawara, S., Droplet deposition and entrainment modeling based on the three-fluid model, the 3rd Int. Nat. Top. Mtg. on Nuclear Reactor Power Plant Thermal Hydraulics and Operations, Seoul, Korea(1988), A1-19 to A1-28.

[7] Sugawara, S. and Miyamoto, Y., FIDAS: Detailed subchannel analysis code based on the three-fluid and three-field model, accepted to Nuclear Engineering & Design -- Special issue for recent Japanese advances in the area of nuclear reactor thermal-hydraulics and related safety.

[8] Sakai, T., Rummence, H.E.C. and Sugawara, S., FIDAS: A three-fluid subchannel code for dryout prediction in rod bundles, the 10th Annual Conf. of CNS, Ottawa (June 1989).

[9] Sugawara, S., Sakai, T., Watanabe, K. and Rummence H.E.C., Subchannel analysis by the FIDAS code based on the three-fluid model, Proceedings of the Fourth International Topical Meeting on Nuclear Reactor Thermal-Hydraulics (NURETH-4), Karsruhe F.R.G., Vol.1, 560-567 (1989).

[10] Hewitt, G.F. and Pulling, D.J., Liquid entrainment in adiabatic steam-water flow, AERE-R5374(1969).

[11] Keeys, R.K.F., Ralph, J.C. and Roberts, D.N., Liquid entrainment in adiabatic steam-water flow at 500 and 1000 p.s.i.a., AERE-R6293(1970).

[12] Yanai, M., Study on boiling heat transfer in a channel, PhD. Thesis of Kyoto University(1971).

[13] Haramura, Y. and Katto, Y., A new hydrodynamic modeling on CHF, Trans. of JSME, 445-B(1983), 1919-1927. (in Japanese)

[14] Bennett, A.W., Hewitt, G.F., Kearsey, H.A., Keeys, R.K.F. and Pulling, D.J., Studies on burnout in boiling heat transfer to water in round tubes with non-uniform heating, AERE-R5076(1966).

[15] Keeys, R.K.F., Ralph, J.C. and Roberts, D.N., The effect of heat flux on liquid entrainment in steam-water flow in a vertical tube at 1000 psia, AERE-R6294(1970).

[16] Tompson B. and Macbeth R.V., Boiling water heat transfer, burnout in uniformly heated round tubes: A compilation of world data with accurate correlations, AEEW-R356(1964).

[17] Bennett, A.W., Hewitt, G.F., Kearsey, H.A. and Keeys, R.K.F., Heat transfer to steam-water mixtures flowing in uniformly heated tubes in which the critical heat flux has been exceeded, AERE-R5373(1967).

[18] Katto, Y., Critical heat flux, Advances in Heat Transfer, 17, Academic Press.Inc.(1985).

[19] Katto,Y., Critical heat flux in boiling, Proc. of 8th Int. Nat. Heat Transfer Conf. vol.1 (1986), 171-180.

[20] Hewitt, G.F., Critical heat flux in boiling, Proc. of 6th Int. Nat. Heat Transfer Conf.,vol.6 (1978), 143-151.

[21] Katto, Y, The calculation of critical heat flux in annular flow regime taking into account the critical liquid film thickness concept, Trans of JSME, Ser.B, vol.50 No.451 (1984), 801-808. (in Japanese)

[22] Hewitt, G.F. et al., Studies on burnout in boiling heat transfer to water in round tubes with non-uniform heating, AERE-R5076(1966).

[23] Lee, D.H., An experimental investigation of forced convection burnout in high pressure water--Part-Ⅲ , AEEW-R355(1965).

[24] Stevens, G.F. et al., An experimental investigation into forced convection burnout in Freon, with reference to burnout in water, AEEW-R321(1964).

[25] Barnett, P.G. and Wood, R.W., An experimental investigation to determine the scaling laws of forced convection boiling heat transfer -- part2: an examination of burnout data for water, Freon 12 and Freon 21 in uniformly heated round

tubes, AEEW-R443(1965).

[26] Becker, K.M. et al., Proc. of Semi. Two-Phase Flow Thermohydraulics, Rome, 51 (1972).

[27] Zuber, N., Staub, F.W. and Bijwaard G., Vapor void fraction in subcooled boiling and in saturated boiling systems, 3rd Int. Heat Transfer Conf.(1966), 5, 24-28.

[28] Lottes, P.A. and Flinn, W.S., A method of analysis of natural circulation boiling systems, Nuclear Science Engineering, 1-6 (1956), 420.

[29] Baker, O., Design of pipe lines for simultaneous flow of oil and gas, Oil and Gas Journal, 26 July (1954).

[30] Morooka, S., Ishizuka, T. and Kagawa, T., Development of POST-MULTI Code for the analysis of heat transfer beyond boiling transition, J. of the Atomic Energy Society of Japan, Vol.26, No.2, 136-138 (1984), (in Japanese).

Table 1 Constitutive Equations

Wall-liquid drag force

$$\tau_{WF} = \bar{A}_{WF} f_{WF} \frac{\rho_F}{2} u_F^2 \text{ , in Pa/m}$$

f_{WF} = Blasius' expression

$$= \frac{1}{4} \left(\frac{0.316}{Re_F^{0.25}}\right) \text{ , dimensionless}$$

Vapor-liquid drag force

$$\tau_{FG} = \bar{A}_{FG} f_{FG} \frac{\rho_G}{2} (u_G - u_F)^2$$

f_{FG} = Wallis' expression

$$= \frac{1}{4} \left(\frac{0.316}{Re_G^{0.25}}\right)\left(1 + 300 \frac{t_F}{D}\right)$$

Vapor-droplet drag force [30]

$$\tau_{EG} = \bar{A}_{EG} K_{EG} \frac{\rho_G}{2} (u_G - u_E)^2$$

$$K_{EG} = \frac{24}{Re_E}(1 + 0.15\, Re_E^{0.687}) + \frac{0.42}{1+4.25\times10^4 Re_E^{-1.16}}$$

Droplet size

$$D_E = \begin{cases} \dfrac{\sigma\, We}{\rho_G (u_G - u_E)^2} \\ 10^{-3} \text{ , if } D_E < 10^{-3} \end{cases}$$

where We = Weber number (=5)

Table 2 Computational Conditions for Analytical Results in Fig.13 (modified from Ref.[21]

Calculation model	Deposition	Entrainment			Onset of annular flow		
	k_D (m/s)	C_{eq} (kg/m³)	m_E(kg/m²s)	m_B(kg/m²s)	χ_{tr}	$\alpha_{G,tr}$	State
Whalley et al.	0.01	Empirical value[1]	——	——	0.01	——	$C=C_{eq}$
Wurtz	0.01	——	Empirical formula[3]	Empirical formula[4]	——	0.8	$C=m_E/k_D$
Levy et al.	0.01	Semi-theoretical prediction[4]	——	——	——	0.8	$C=C_{eq}$
Present Analysis	Eq.(3)	——	Eq.(6)	Eq.(12)	——	Eq.(13)	Eq.(15))

Table 3 CHF Data for Sensitivity Analysis

	Run No.	P (MPa)	G (kg/m²s)	D (mm)	H_{sub} (kJ/kg)	l_B (m)	x_{cr} (-)	q_{cr} (MW/m²)
Case-1	TM-590	7.0	2000	10.8	286.1	1.01	0.268	2.243
Case-2	WZ-404	7.0	2000	10.0	52.65	1.51	0.425	1.762
Case-3	WZ-469	7.0	2000	10.0	52.65	7.53	0.592	0.569

(Case-1 is quoted from Tompson-Macbeth[16], and Case-2&3 are from Wurtz[3])

Table 4 Summary of Sensitivity Analysis Results on CHF Prediction

Uncertainty		Variation of CHF (%)		
Parameter	Variation	Case 1	Case 2	Case 3
Measured CHF, $q_{c,meas}$ (MW/m²)		2.243	1.762	0.569
Predicted CHF, $q_{c,cal}$ (MW/m²)		2.243	1.713	0.579
(Measured CHF)/(Predicted CHF)		1.000	1.029	0.982
Liquid film/Vapor shear stress, τ_{FG}	×0.8	0.0	0.0	0.20
	×1.2	0.0	−0.10	−0.39
Droplet/Vapor shear stress, τ_{EG}	×0.8	0.0	0.0	0.0
	×1.2	0.0	0.0	0.0
Liquid film/Wall shear stress, τ_{FW}	×0.8	0.0	1.54	3.34
	×1.2	0.0	−1.44	−2.85
Entrainment rate by roll wave, m_E	×0.8	0.60	2.26	5.80
	×1.2	−0.40	−2.26	−5.40
Entrainment rate by vaporization, m_B	×0.8	0.0	0.62	3.93
	×1.2	−0.5	−0.72	−3.73
Droplet deposition rate, m_D	×0.8	−0.7	−2.26	−16.80
	×1.2	0.7	2.37	16.31
Critical Weber number, We	1.0	0.0	0.0	0.0
	10.0	0.0	0.0	0.0
Transition void fraction, $\alpha_{G,tr}$	−0.05	−2.15	−1.95	−0.88
	+0.05	2.65	2.55	0.88
Initial entrainment fraction, $\alpha_{E,ini}$	10^{-2}	0.10	0.10	0.0
	10^{-4}	0.10	0.10	0.0
Critical film thickness, $t_{F,c}$	×0.8	−4.7	−5.04	0.0
	×1.2	4.3	3.91	0.0

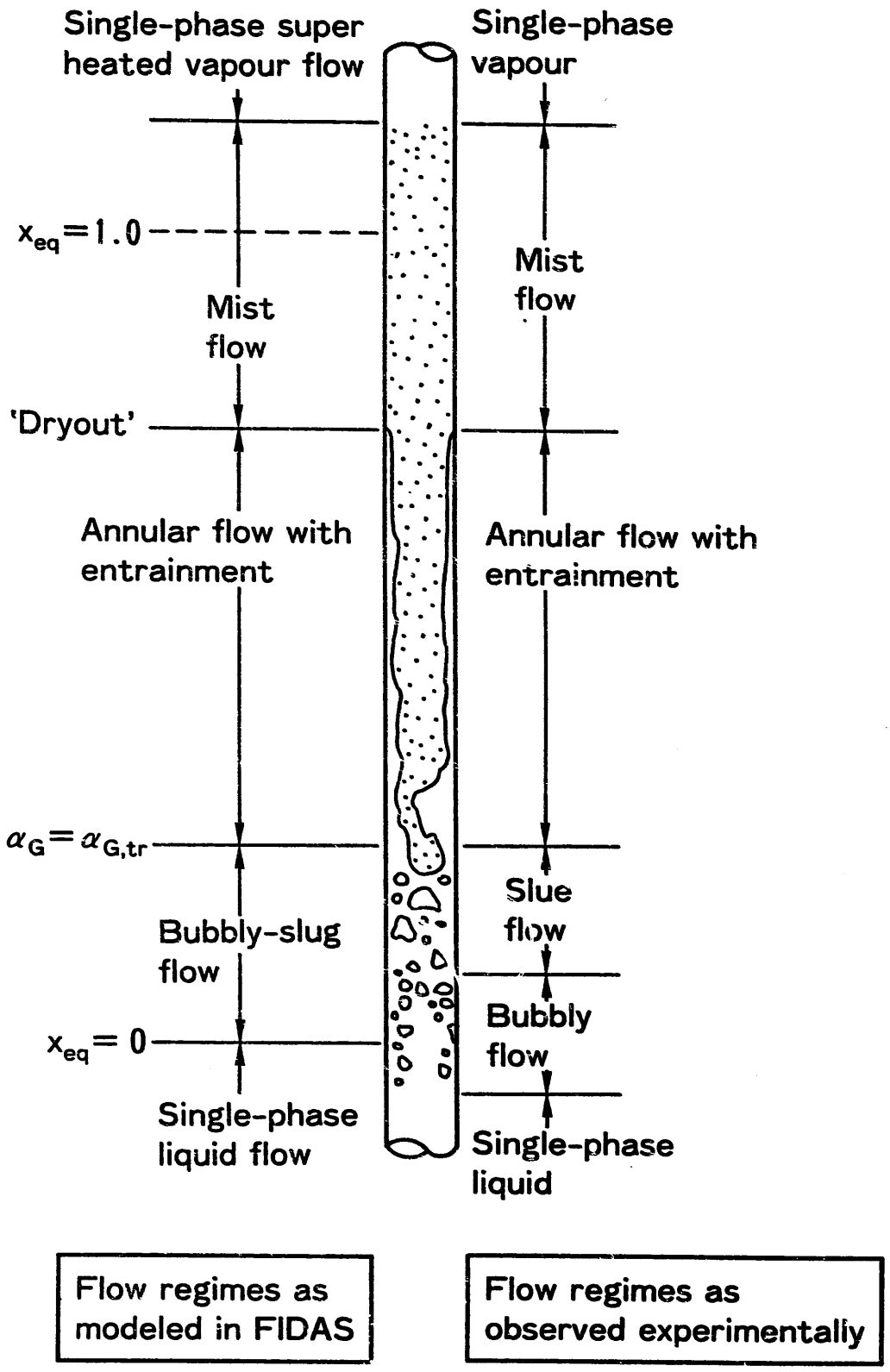

Fig.1 Schematic Representation of Flow Patterns in A Heated Channel

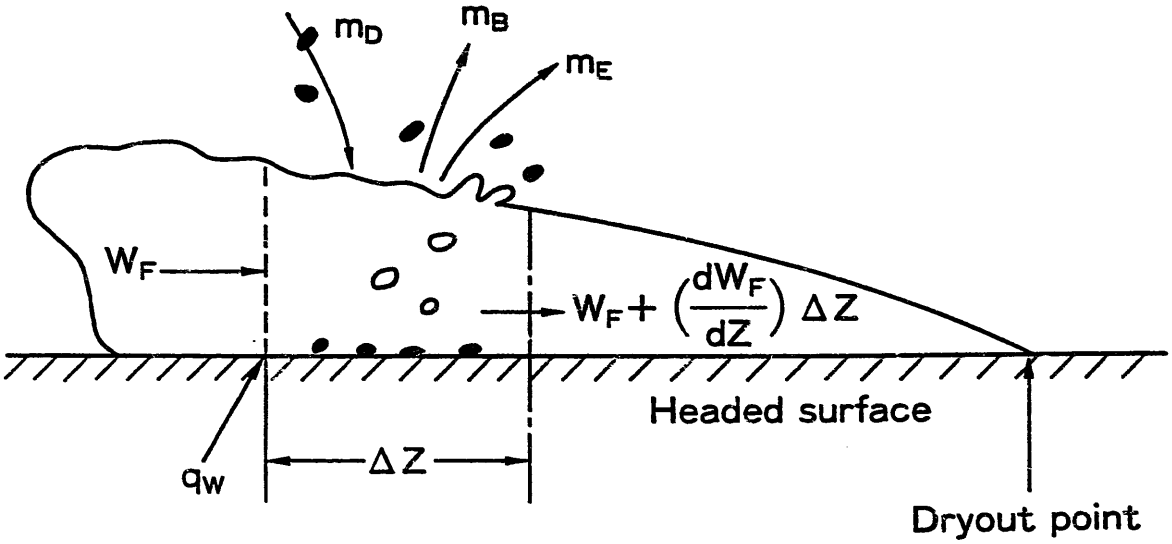

Fig.2 Film Dryout Model in FIDAS Code

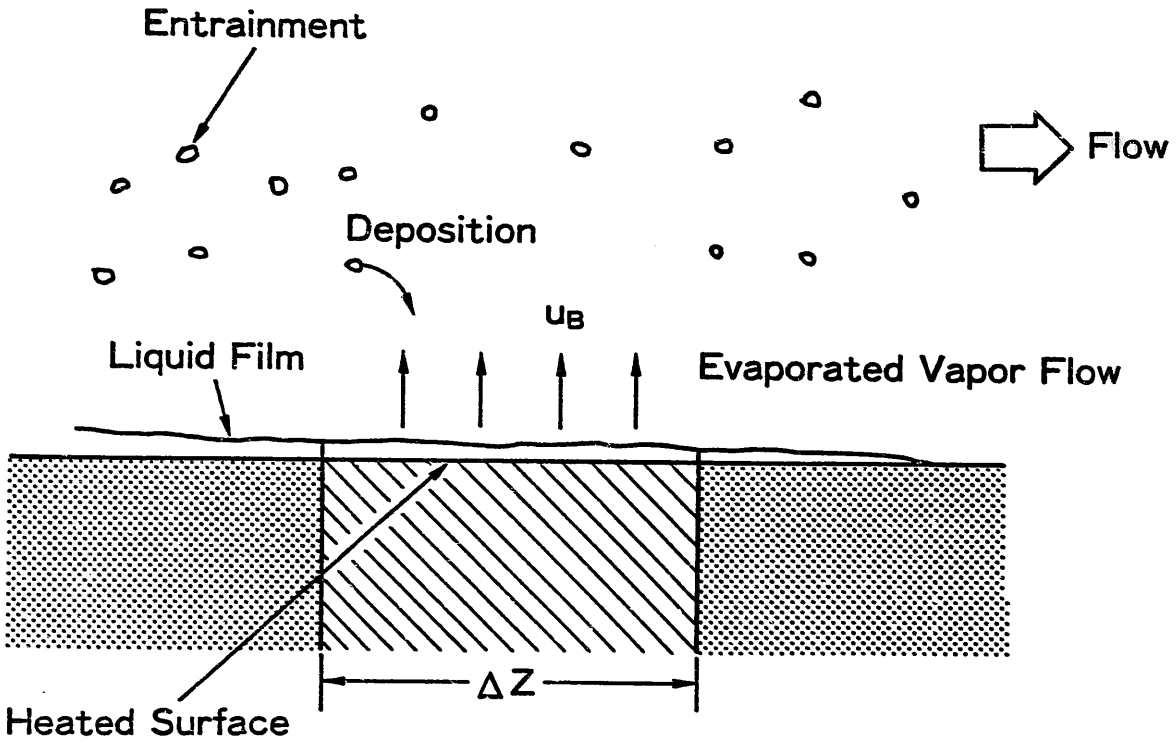

Fig.3 Schematic Model of Deposition Suppression due to Evaporated Vapor Flow

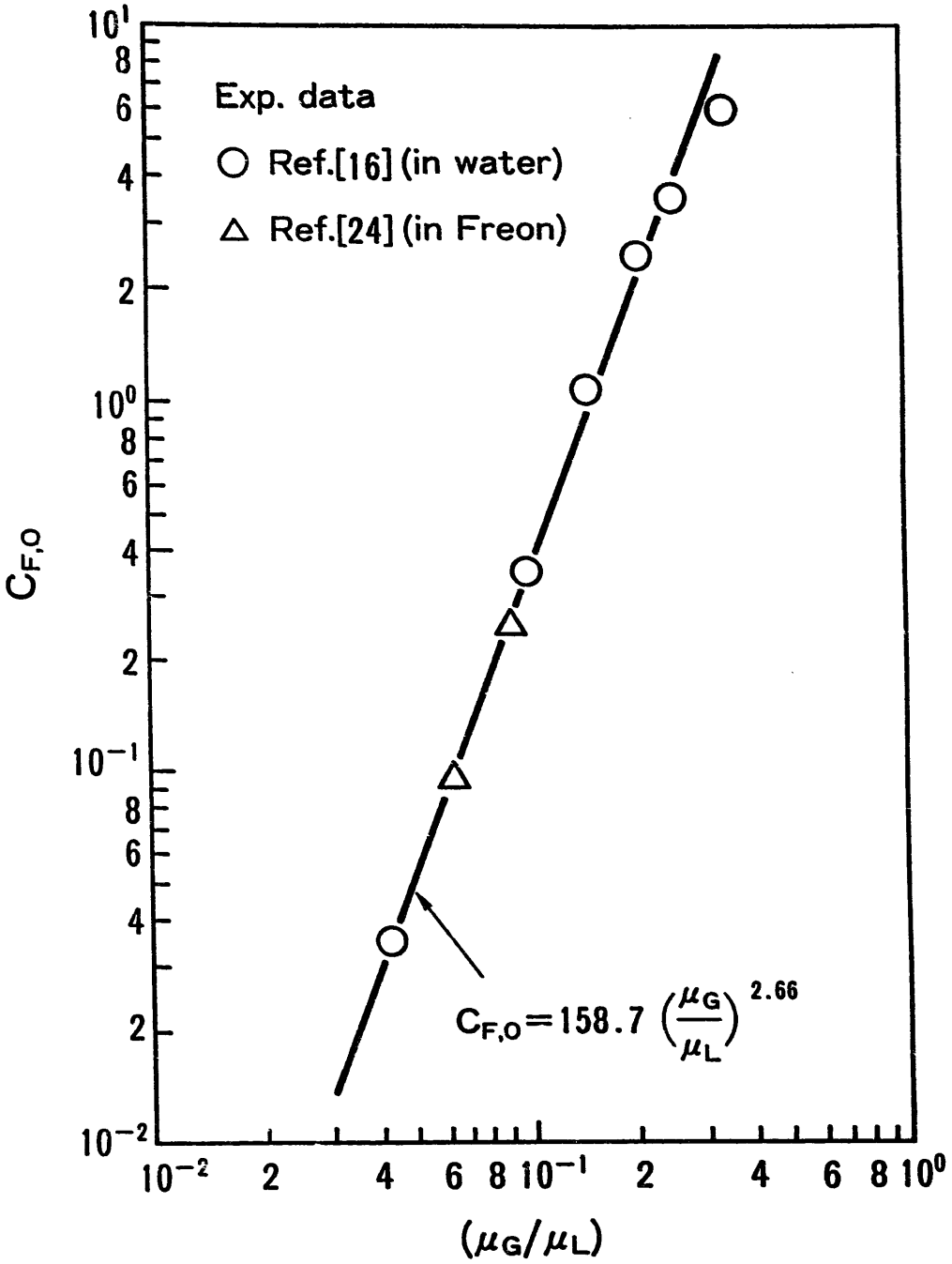

Fig.4 Value of Empirical Constant $c_{F,o}$

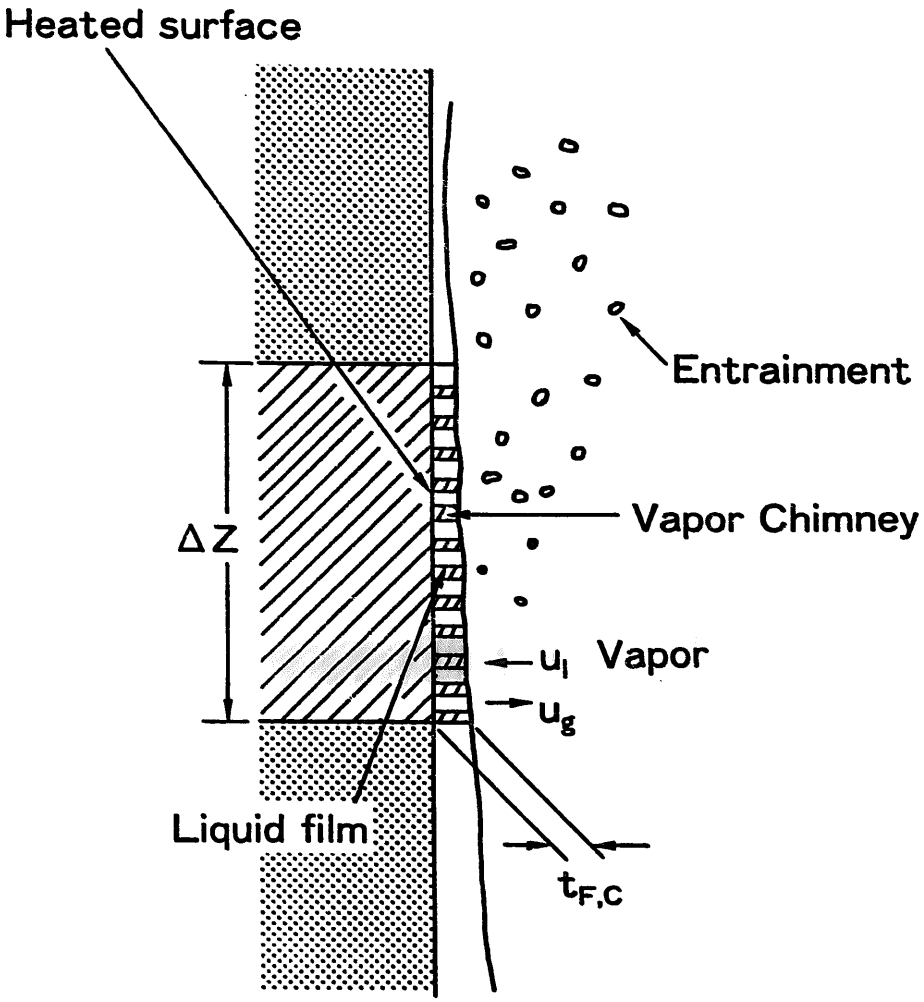

Fig.5 Schematic Model of Liquid Film with Vapor Chimney (quoted from Ref.[13])

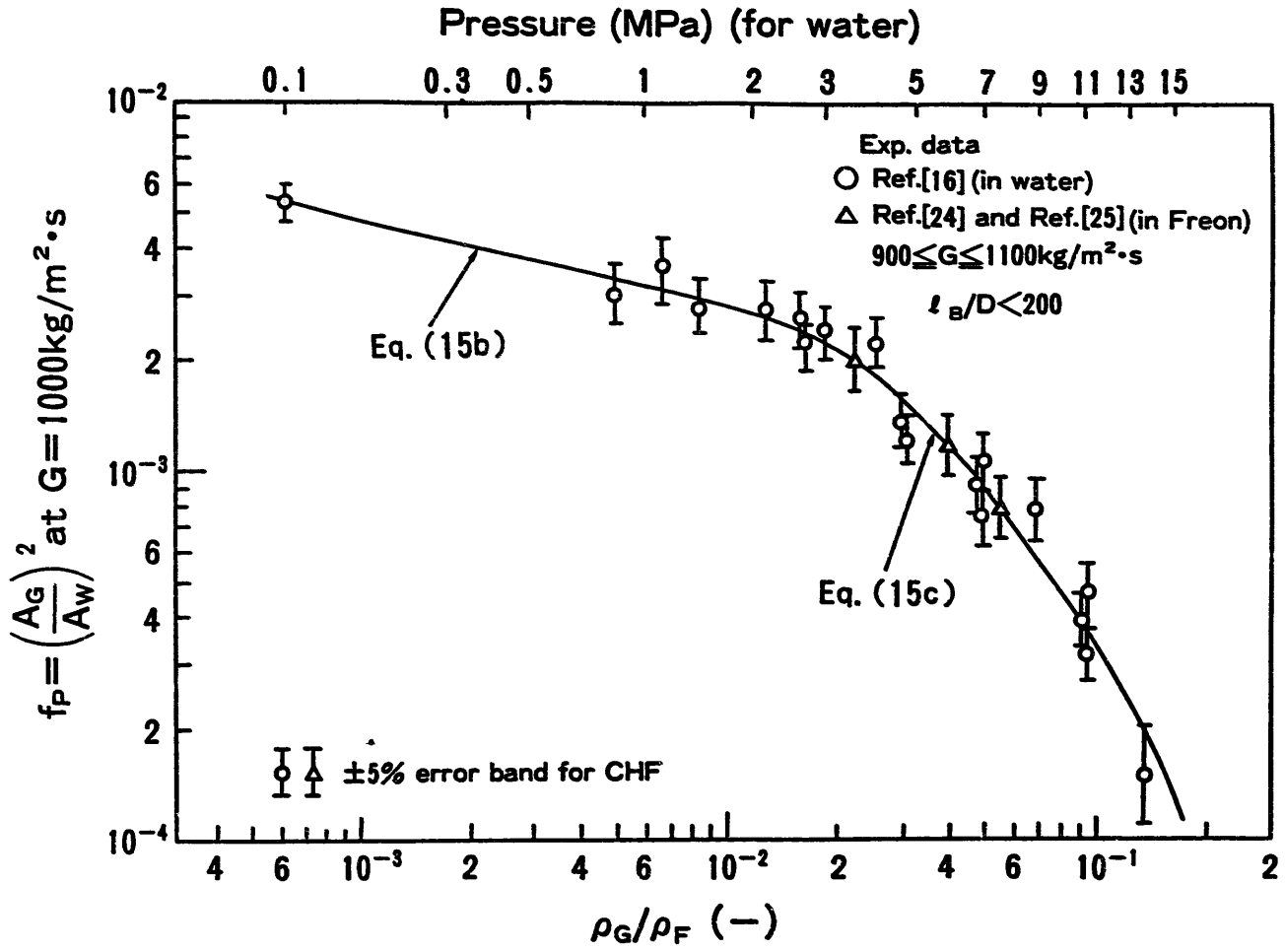

Fig.6(a) Empirical Constant for Maximum Film Thickness Limitation (1)

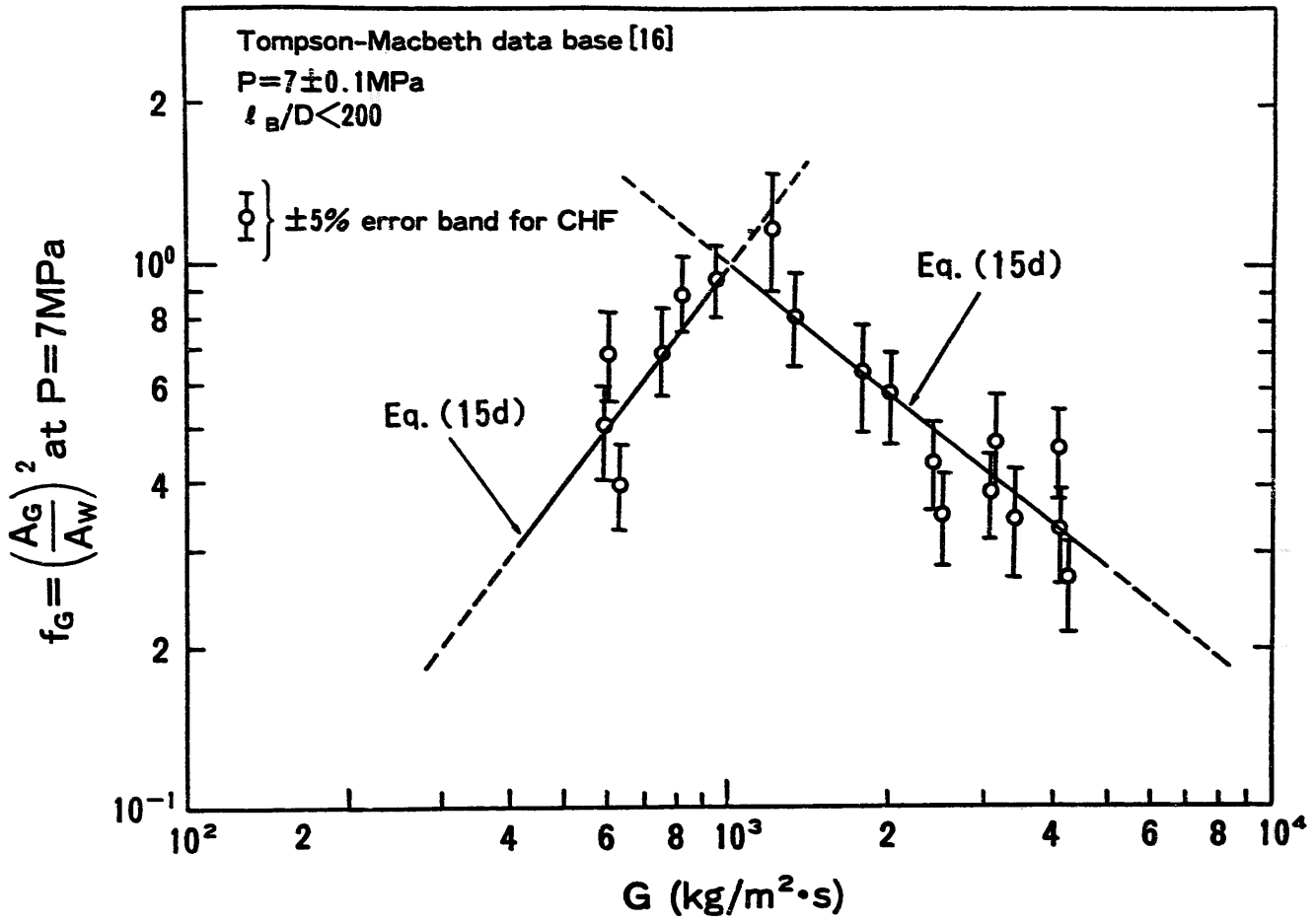

Fig.6(b) Empirical Constant for Maximum Film Thickness Limitation (2)

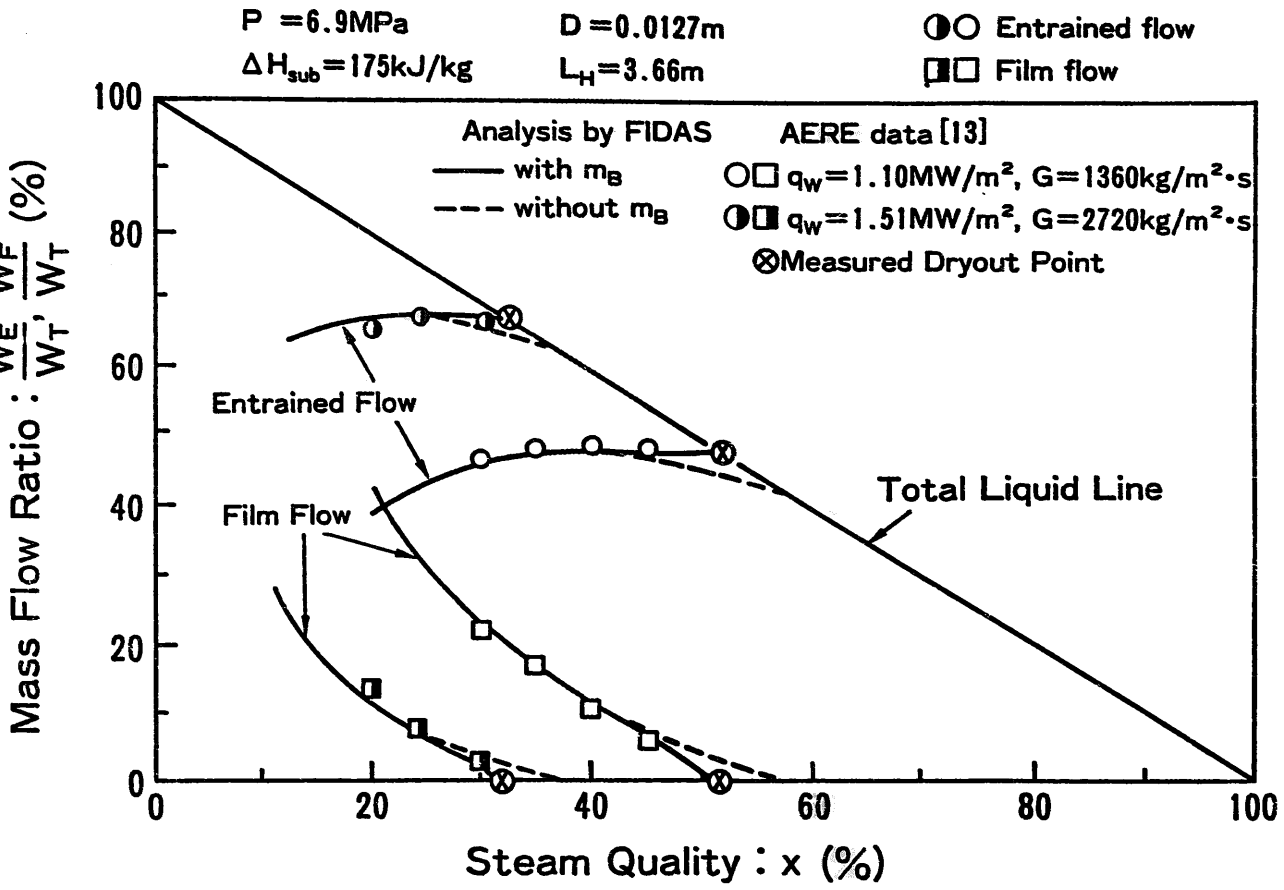

Fig.7 Comparison of Film Flow Variation and Dryout between FIDAS and Experiment

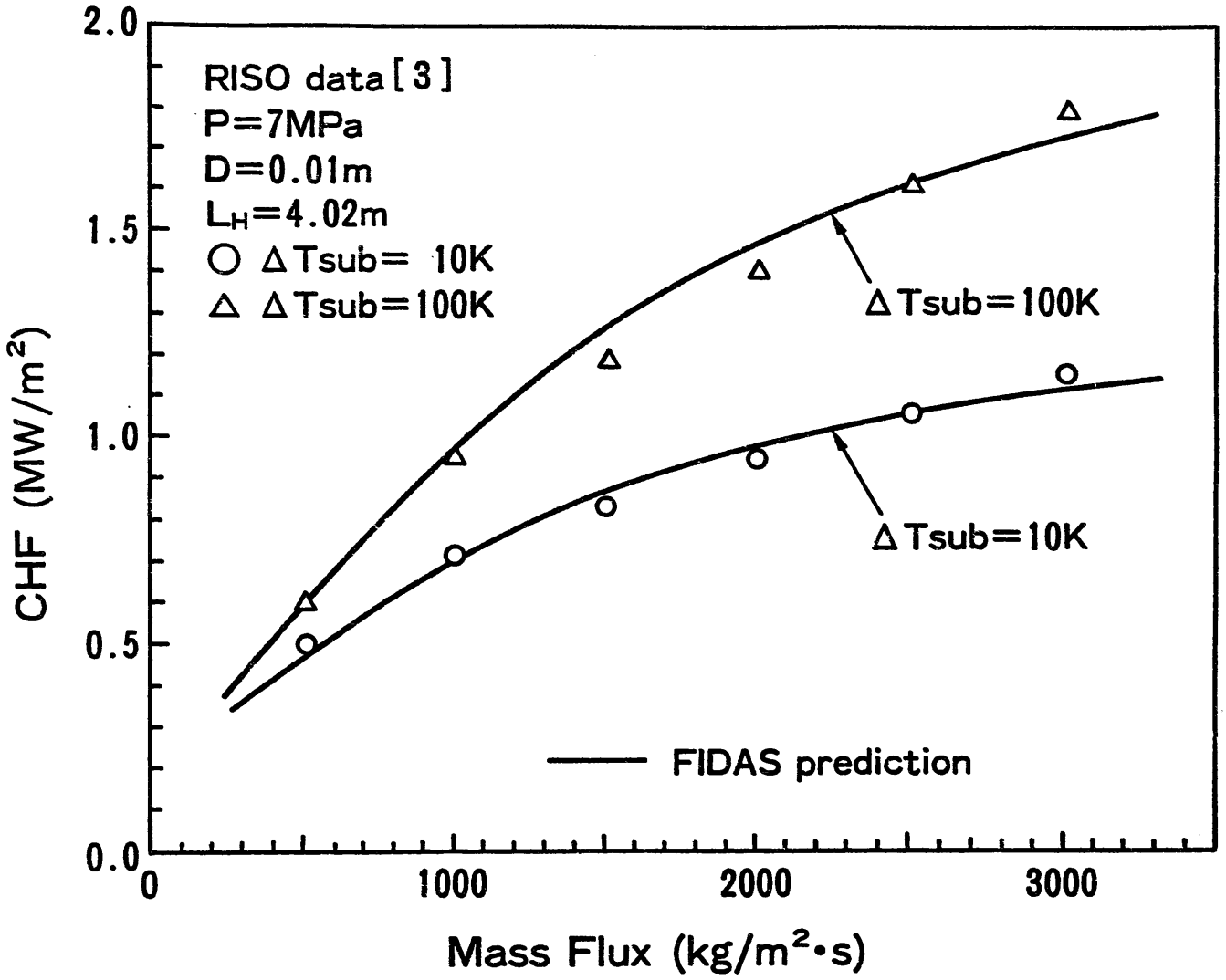

Fig.8 Comparison between Predicted and Measured CHF in q_{cr} vs. G Plane (Effect of Mass Velocity and Inlet Subcooling)

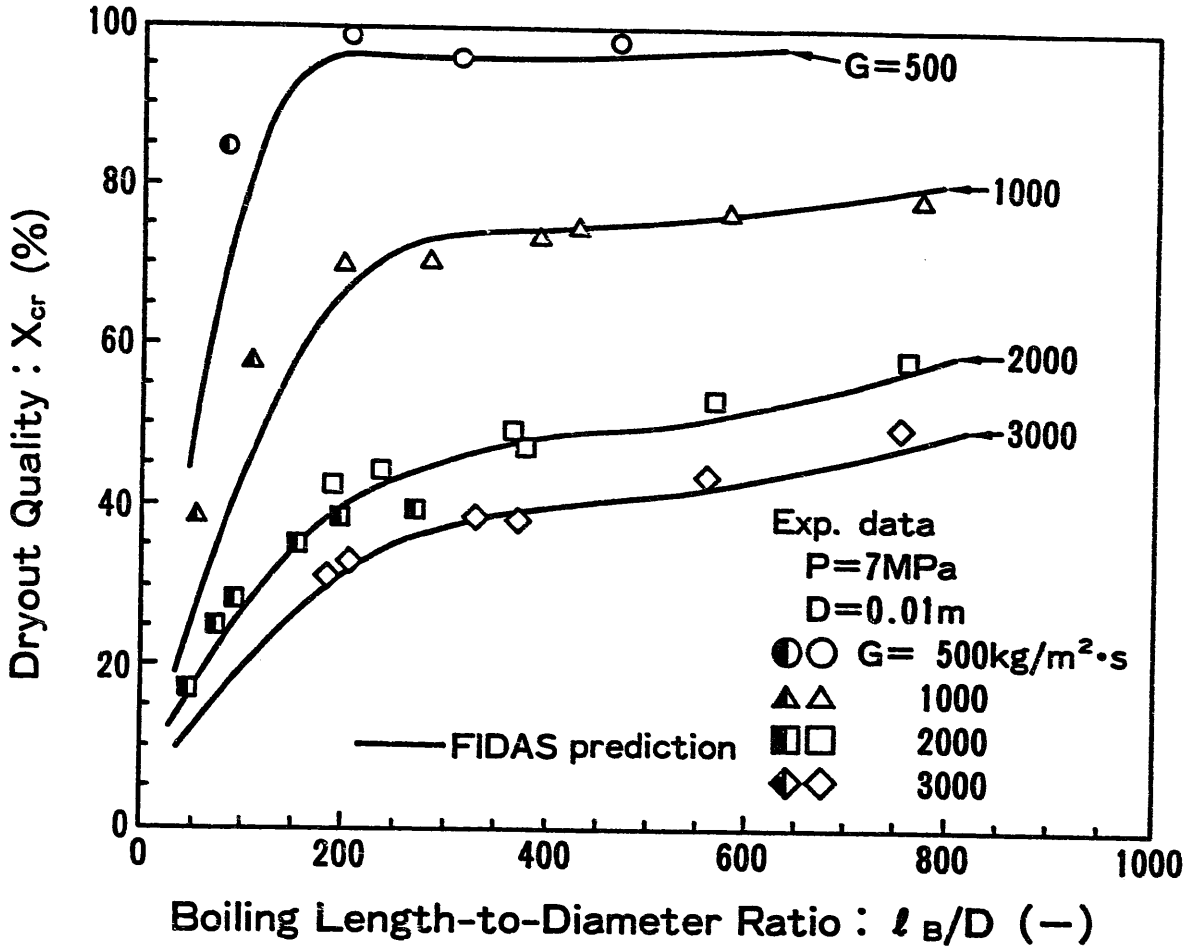

Fig.9 Comparison between Predicted and Measured Dryout Limitation in x_{cr} vs. l_B/D Plane
(Effects of Mass Velocity and Boiling Length)
○△□◇: Ref.[16], D=10.8mm, l_H=0.43-3.05m
◐◭◧◆: Ref.[3], D=10.0mm, l_H=2.02-8.00m

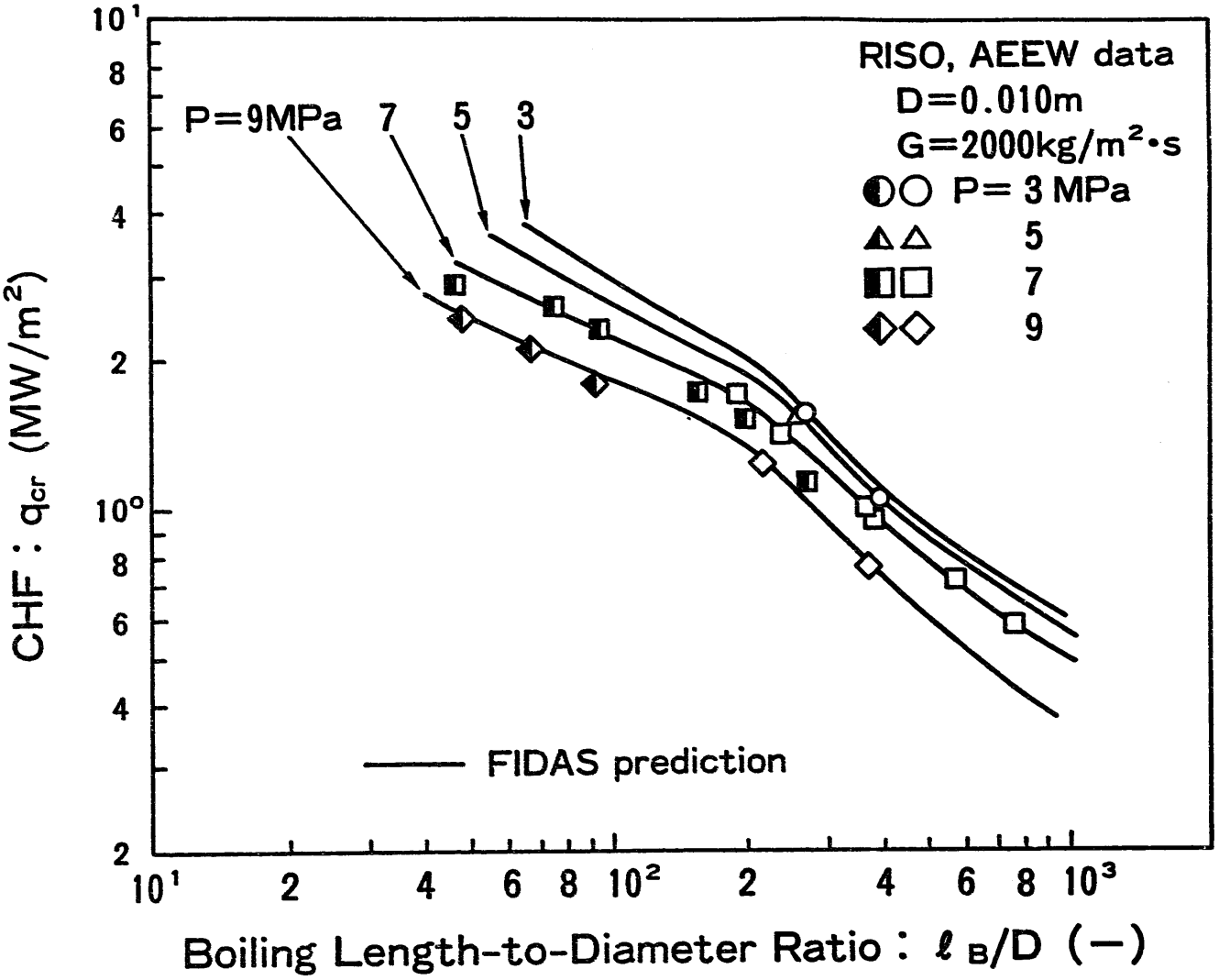

Fig.10 Comparison between Predicted and Measured CHF (Effect of Pressure; data base are same as Fig.9)

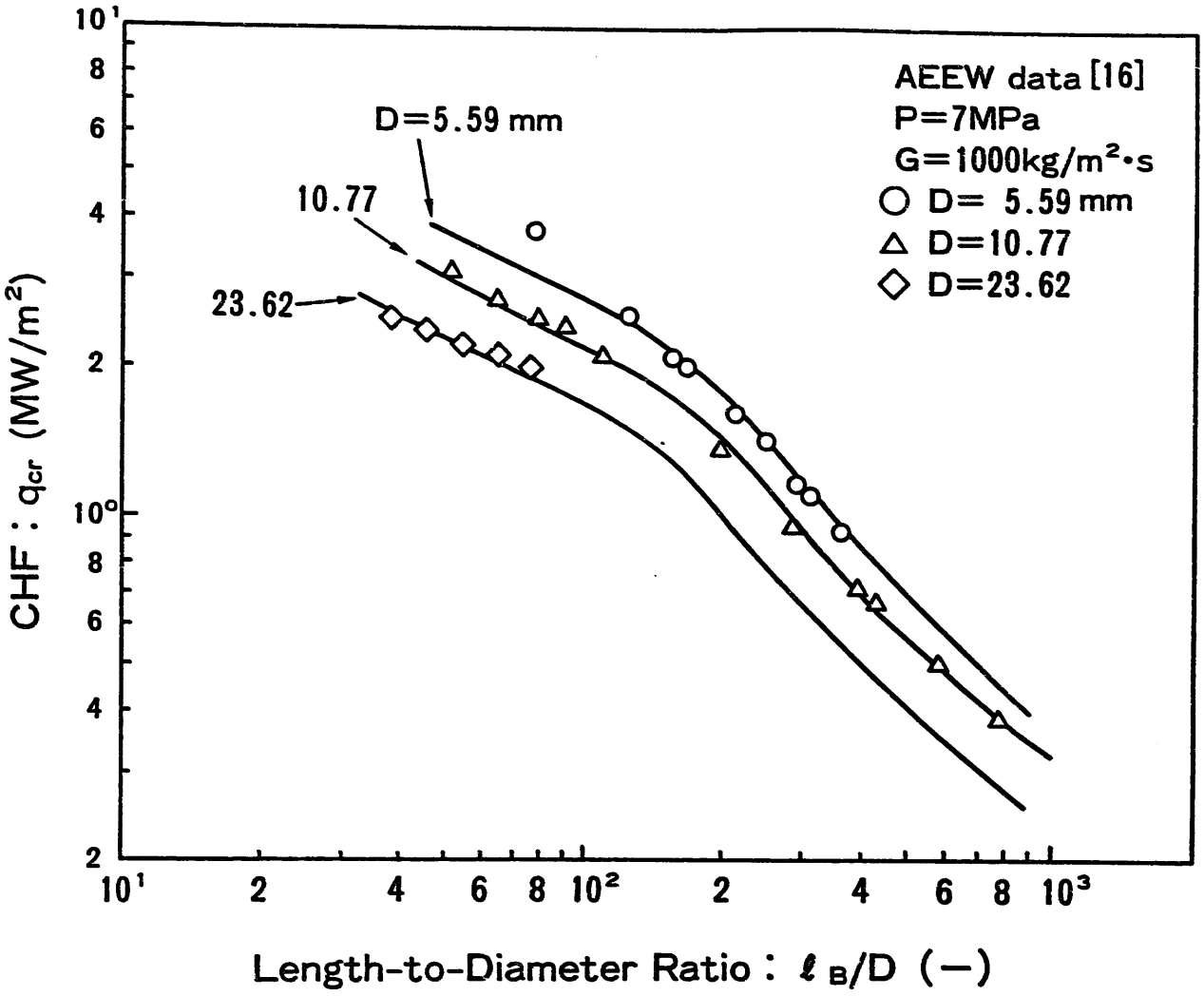

Fig.11 Comparison between Predicted and Measured Effect of Diameter on CHF

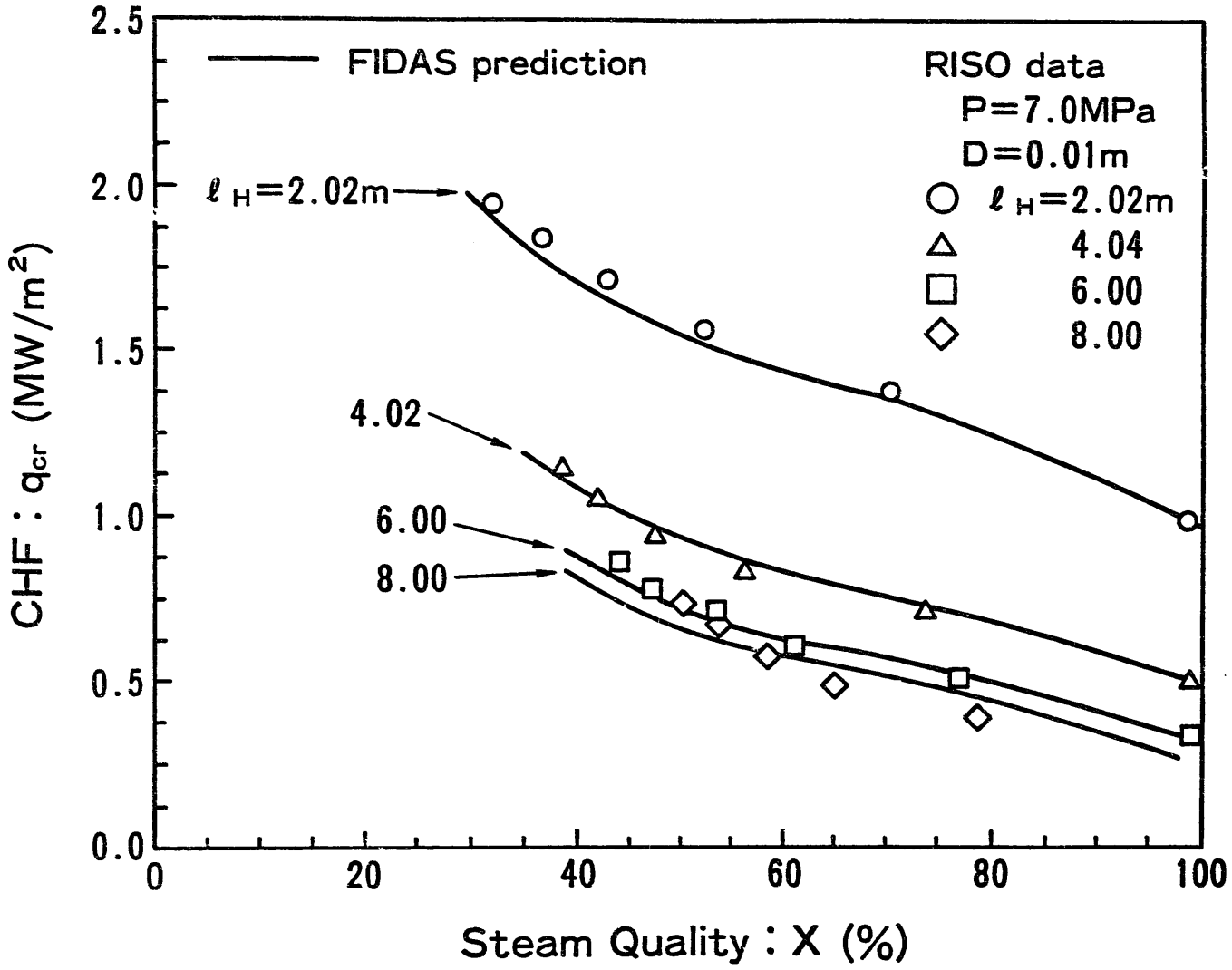

Fig.12 Comparison between Predicted and Measured CHF in q_{cr} vs. x_{eq} Plane (Effect of Heated Length)

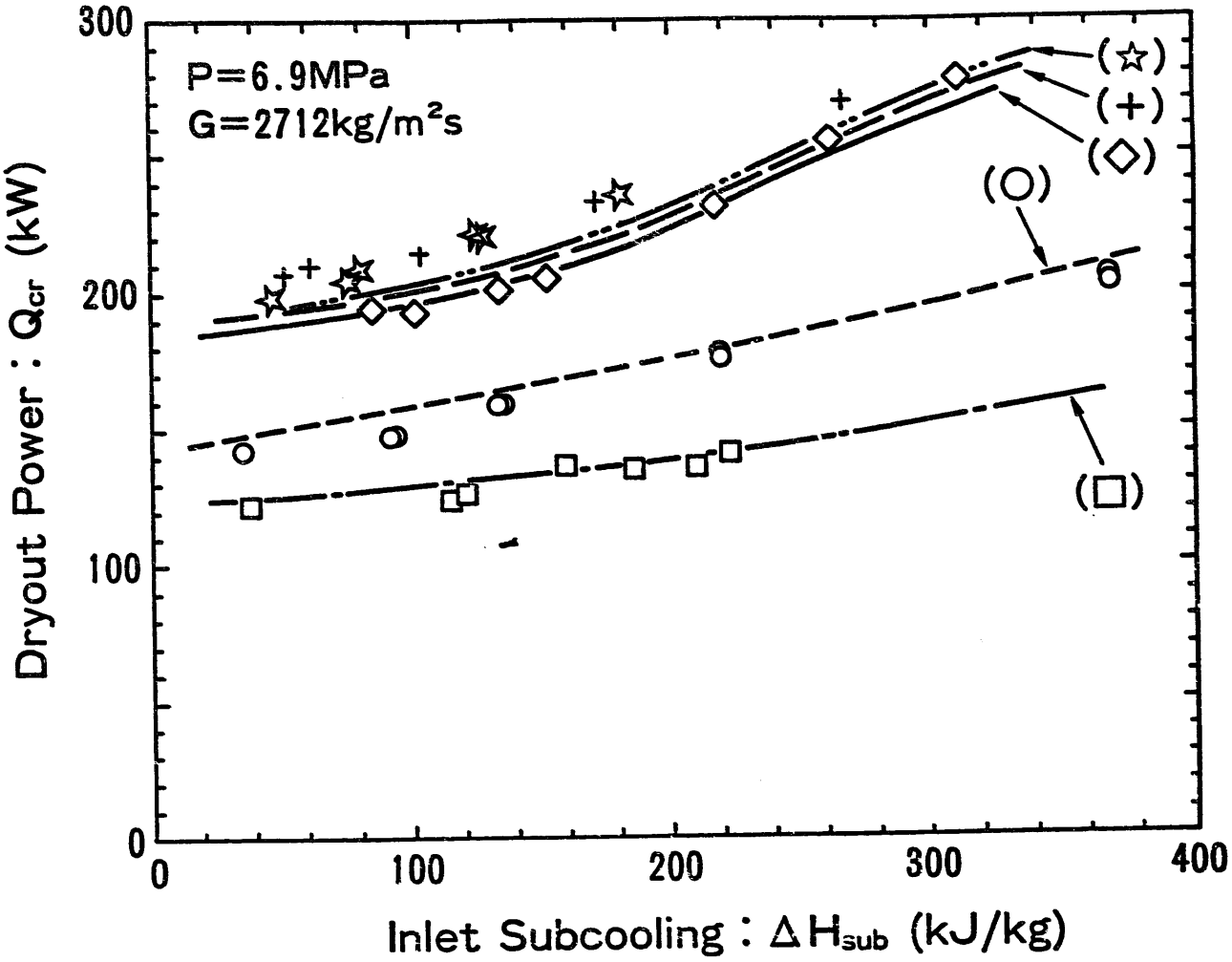

Fig.13 Comparison between Predicted and Measured Dryout Power with Various Type of Axial Power Distributions

AERE-R5076[22]	□AEEW-R355[23]	○AERE-R356[16]
l_H= 3.658m	l_H= 3.658m	l_H= 3.658m
D = 12.57mm	D = 9.47mm	D = 10.82mm
Inlet peaked	Cosine(APF=1.40)	Uniform

◇ q_{max}/q_{min}=3.73
+ q_{max}/q_{min}=2.99
☆ q_{max}/q_{min}=1.91

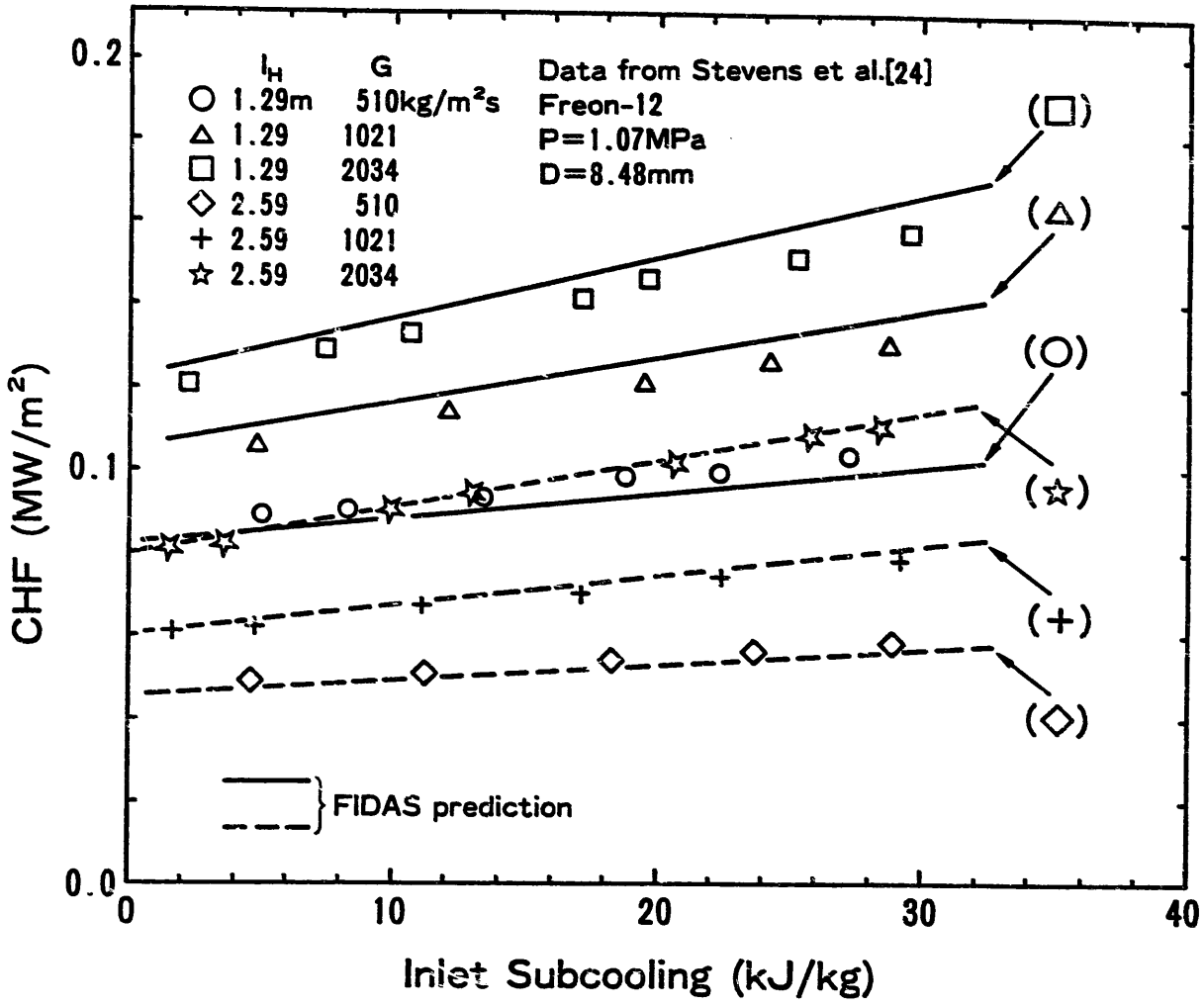

Fig.14 Comparison between Predicted and Measured CHF for Freon-12

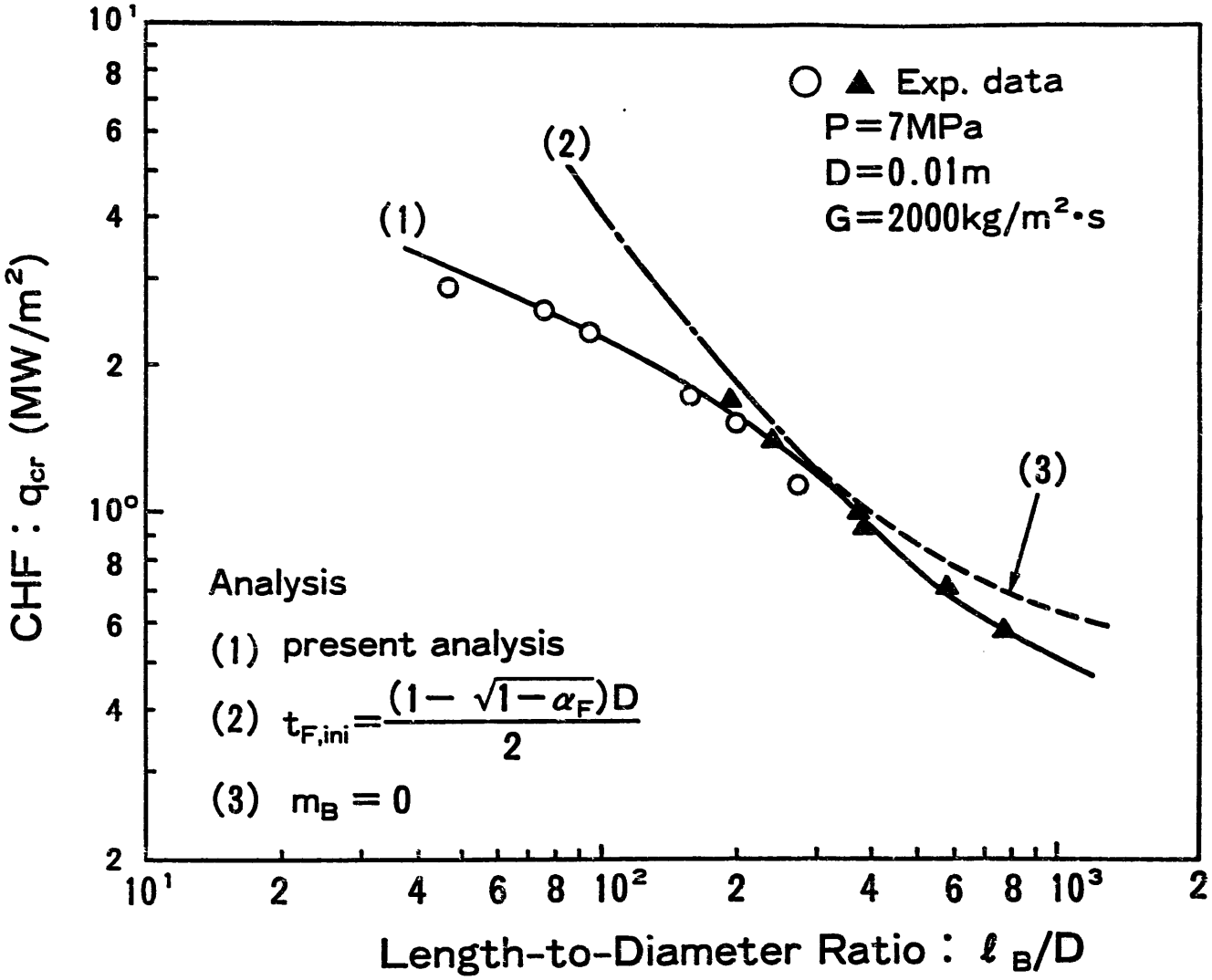

Fig.15 Effect of $t_{F,cr}$ and m_B on CHF Prediction (data base are same as Fig.9)

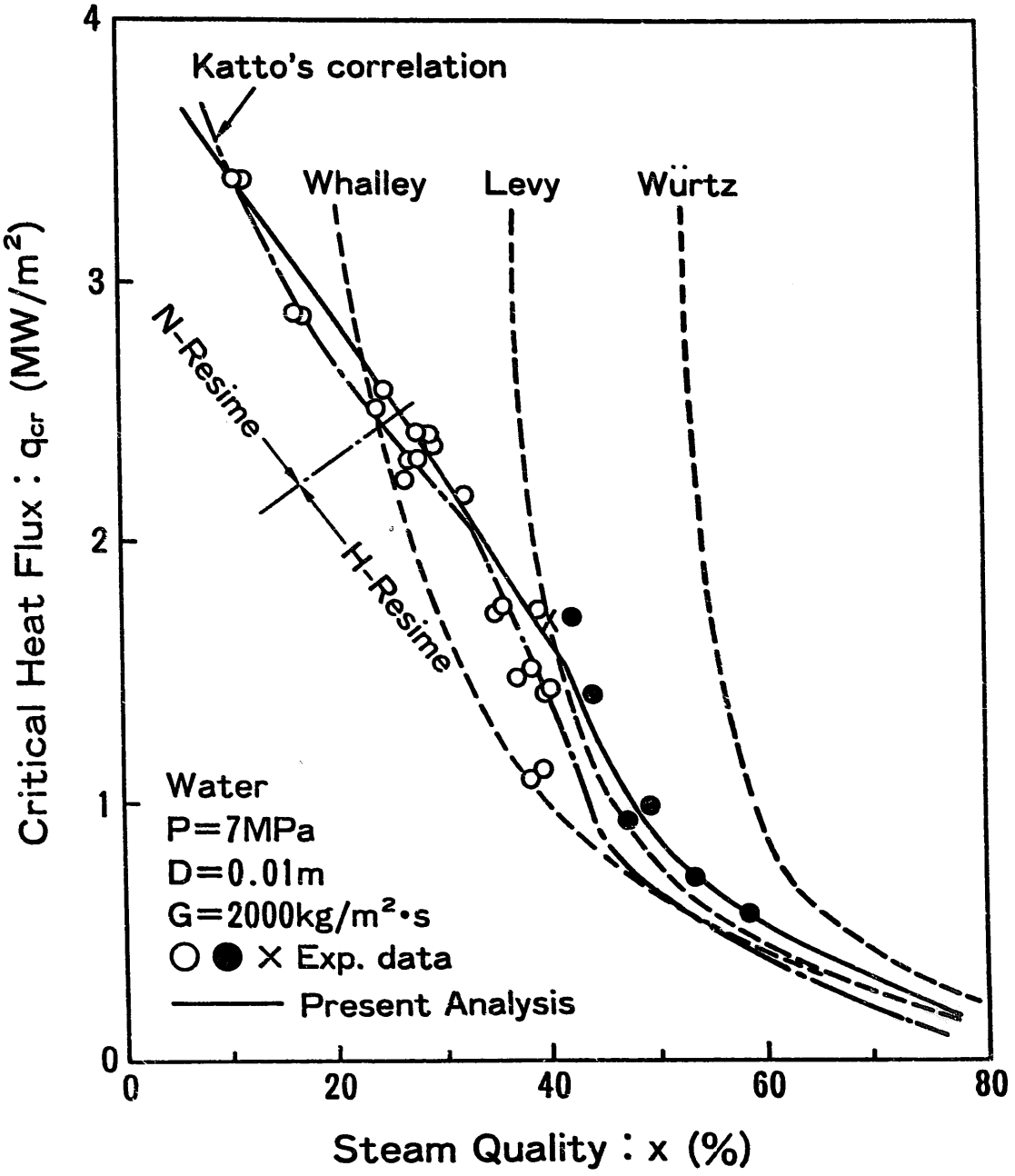

Fig.16 Comparison between Present Analysis and Other Correlations (modified from Ref.[21])

〔○ : Ref.[16], P=6.7-7.1MPa, D=10.8mm, l_H=0.43-3.05m
● : Ref.[3], P=7.0MPa, D=10.0mm, l_H=2.02-8.00m
× : Ref.[26], P=7.0MPa, D=10.0mm, l_H=2.0m〕

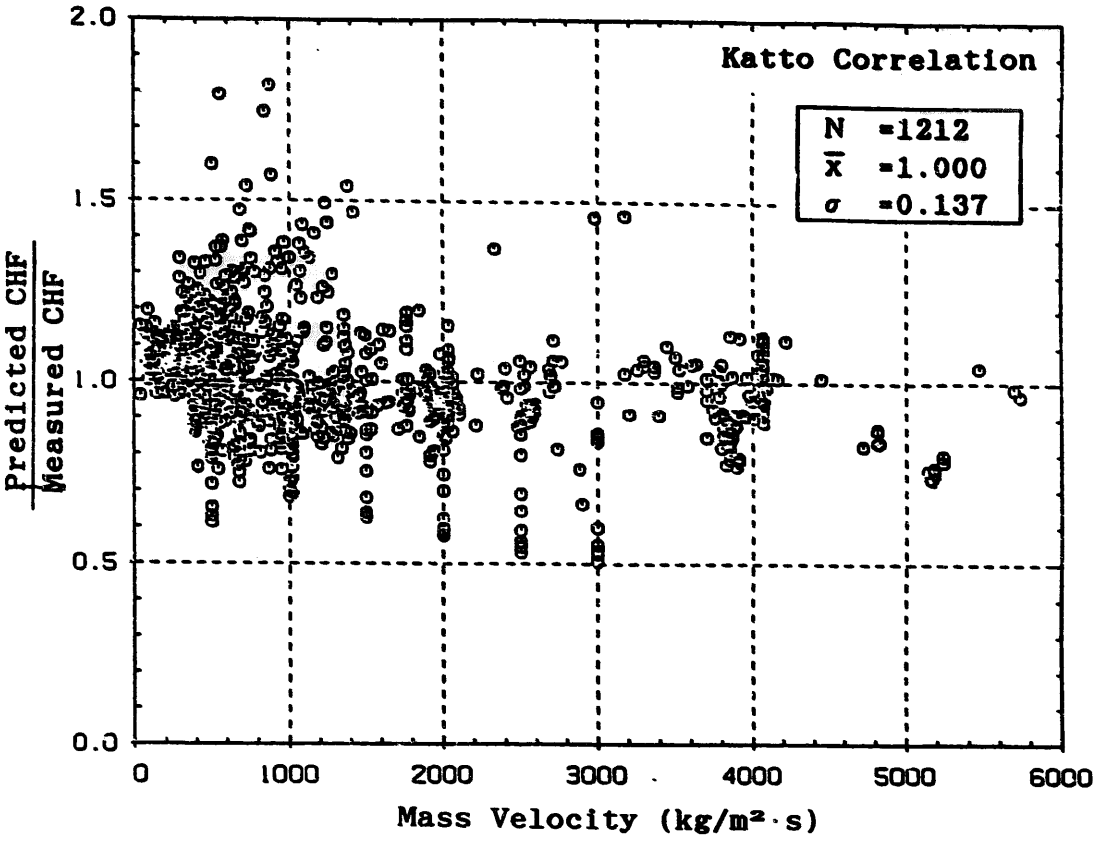

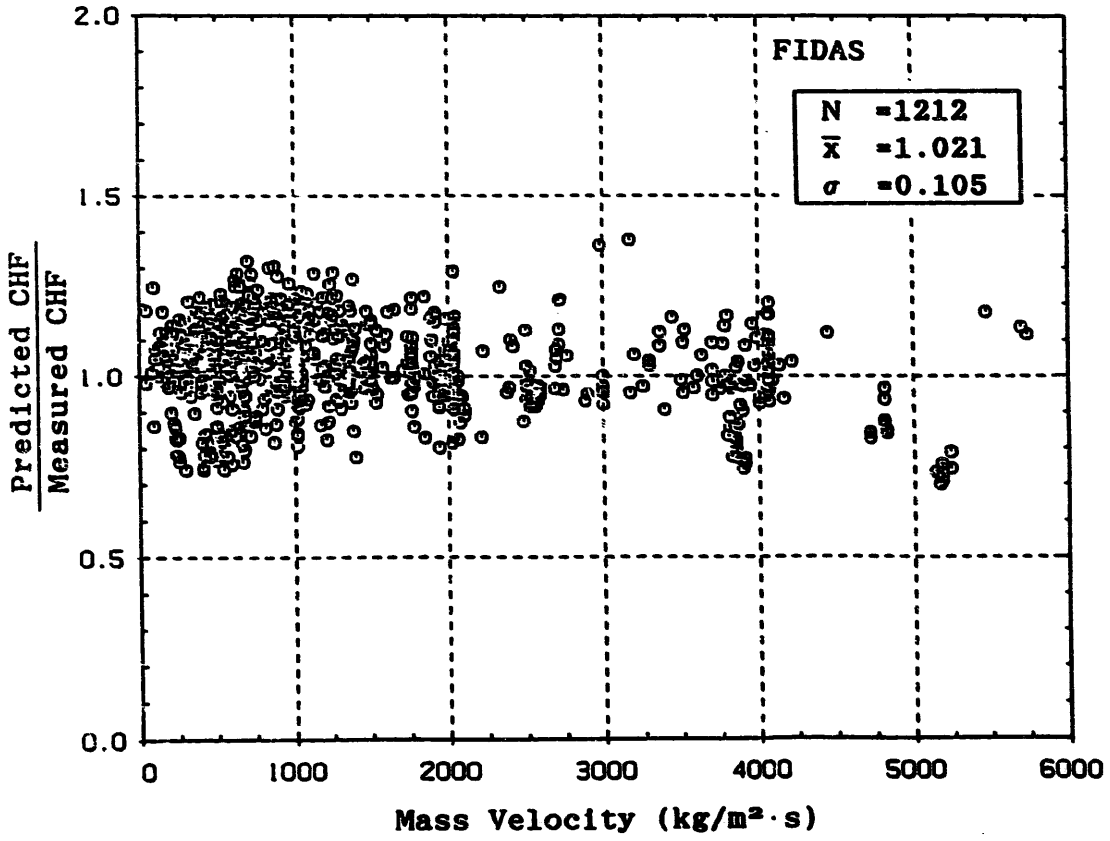

Fig.17 Examination of CHF Prediction Capability comparing with Katto's Correlation (#1: Dependence of CHF on Mass Velocity)

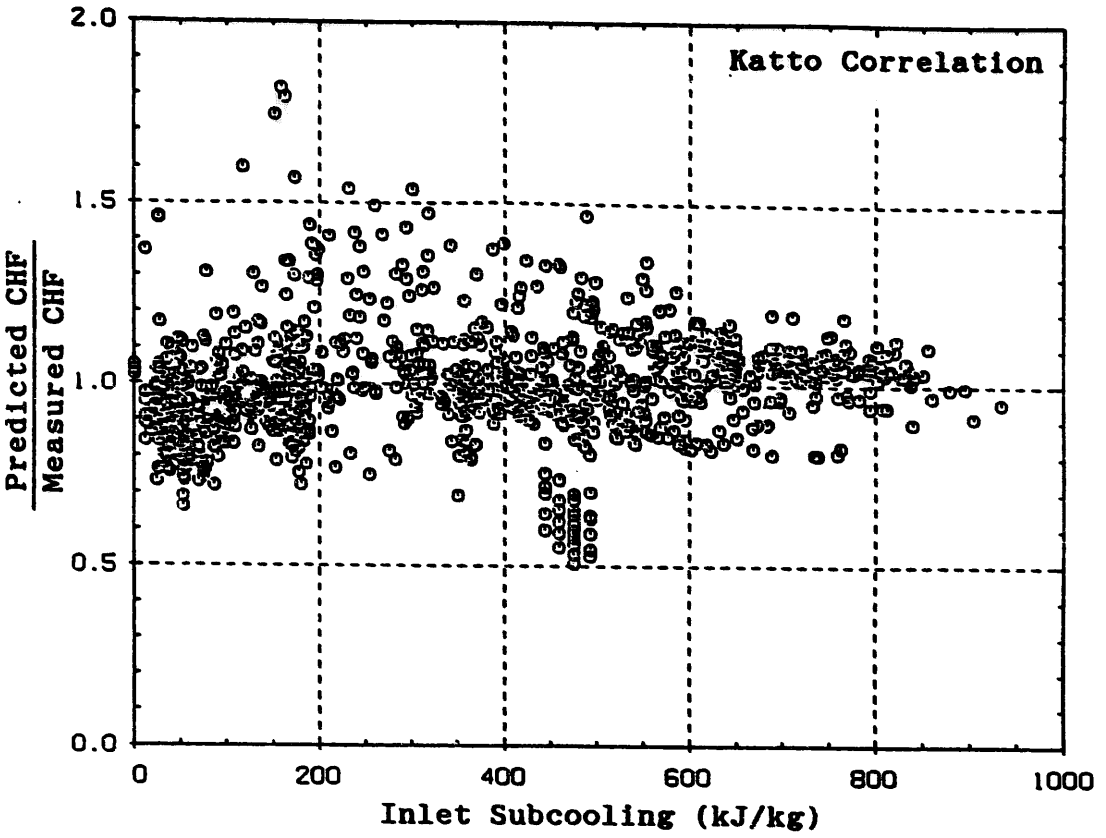

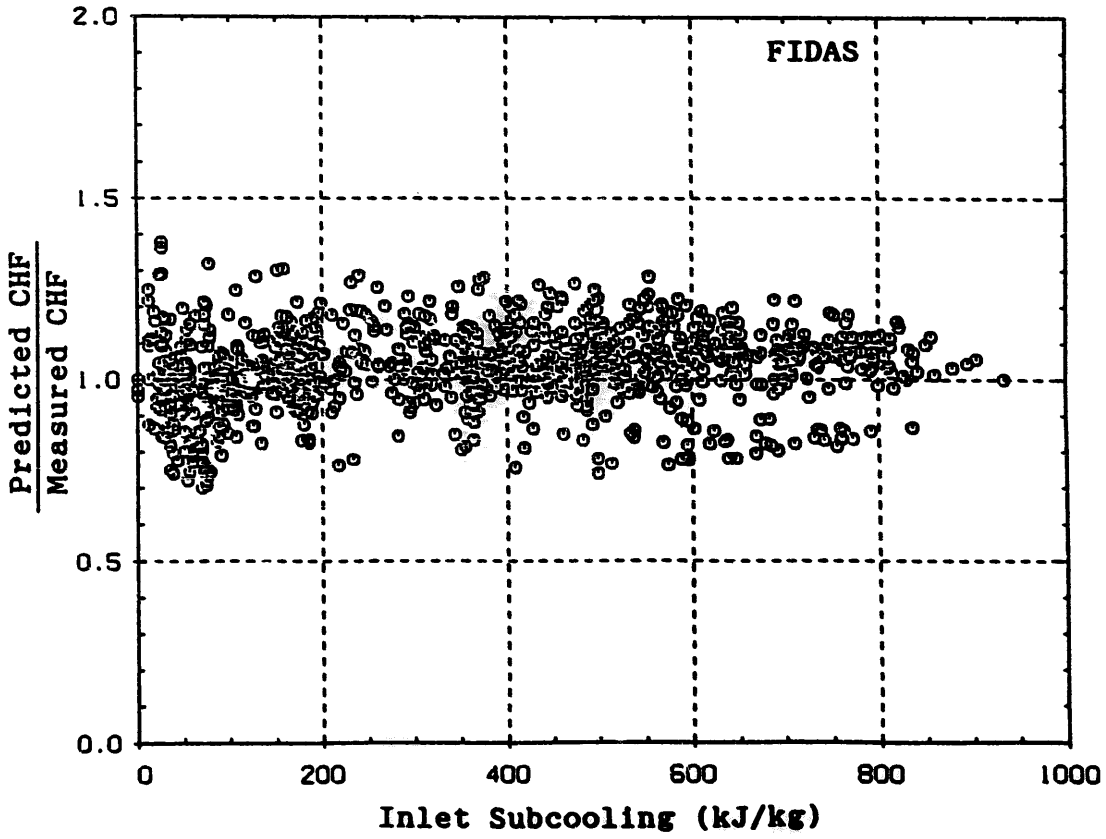

Fig.18 Examination of CHF Prediction Capability comparing with Katto's Correlation (#2: Dependence of CHF on Inlet Subcooling)

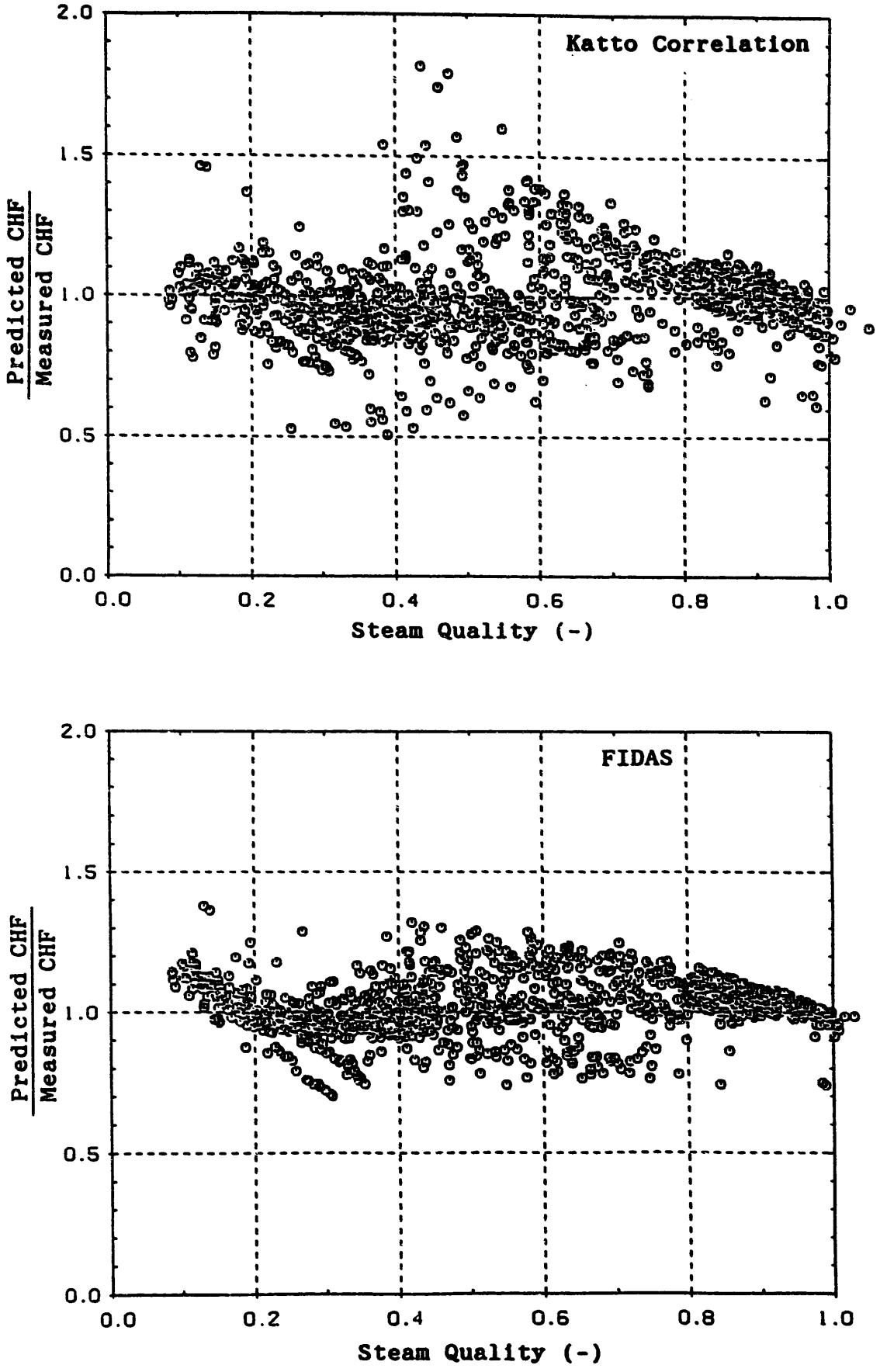

Fig.19 Examination of CHF Prediction Capability comparing with Katto's Correlation (#3: Dependence of CHF on Steam Quality)

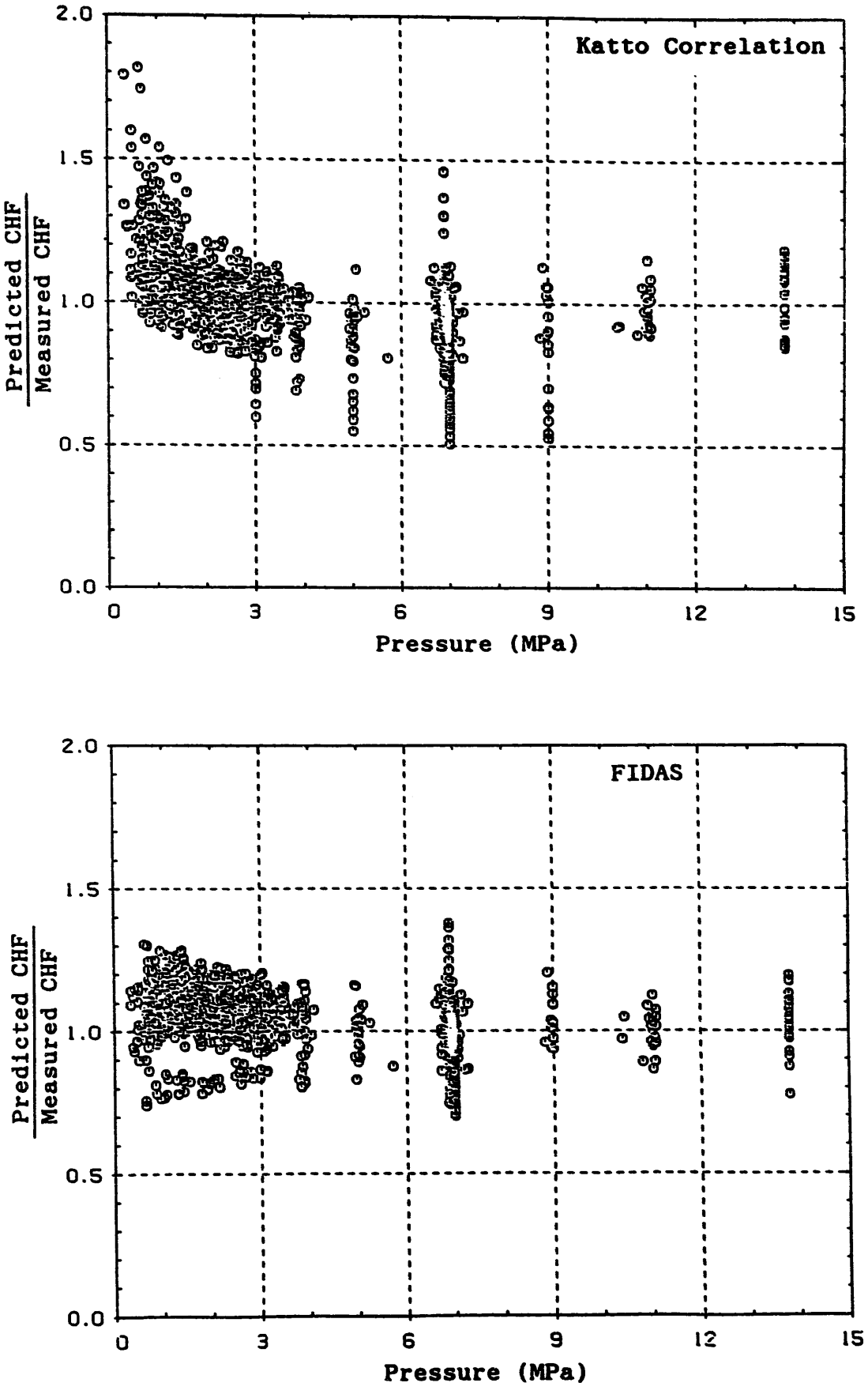

Fig.20 Examination of CHF Prediction Capability comparing with Katto's Correlation (#4: Dependence of CHF on Pressure)

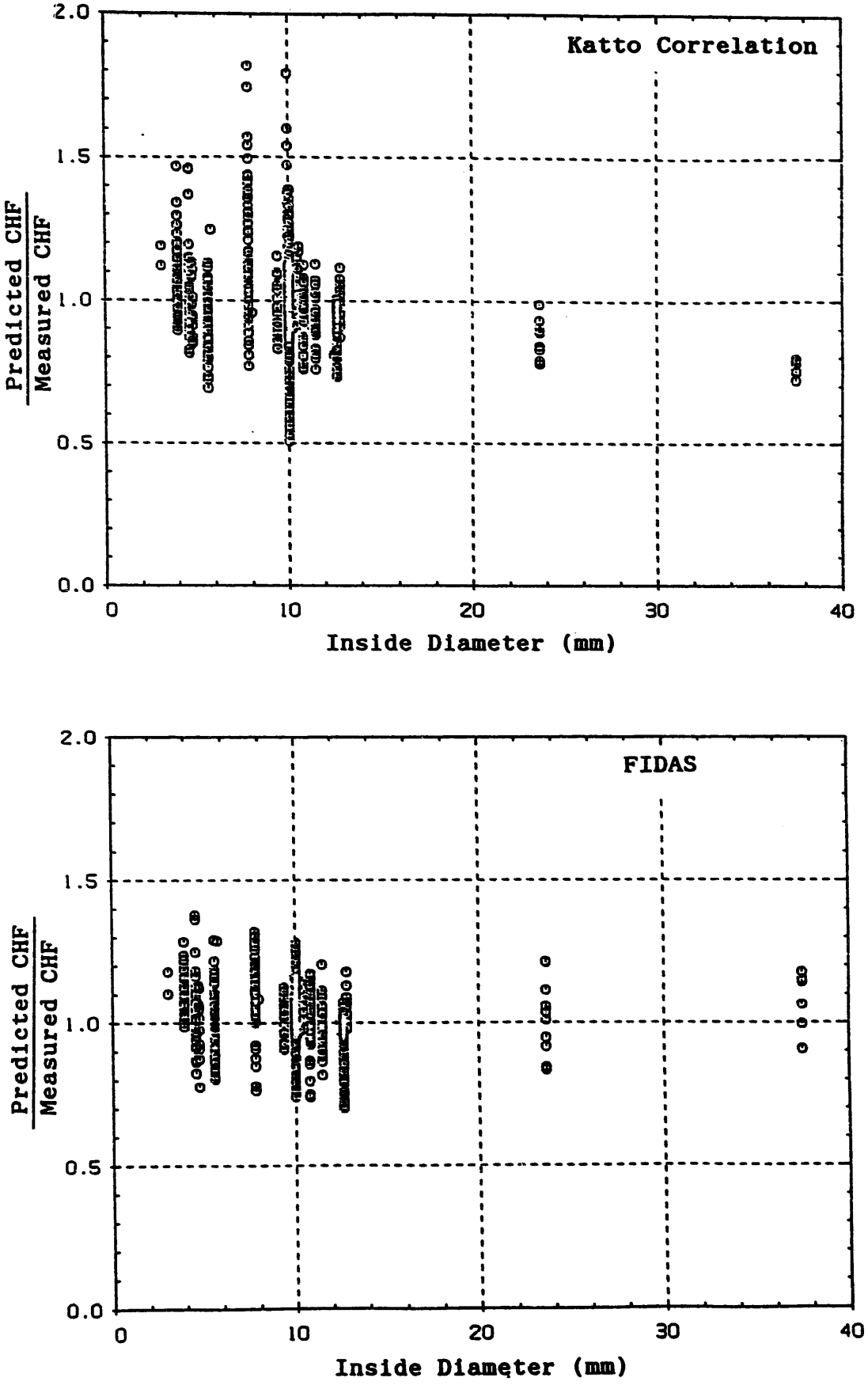

Fig.21 Examination of CHF Prediction Capability comparing with Katto's Correlation (#5: Dependence of CHF on Inside Diameter)

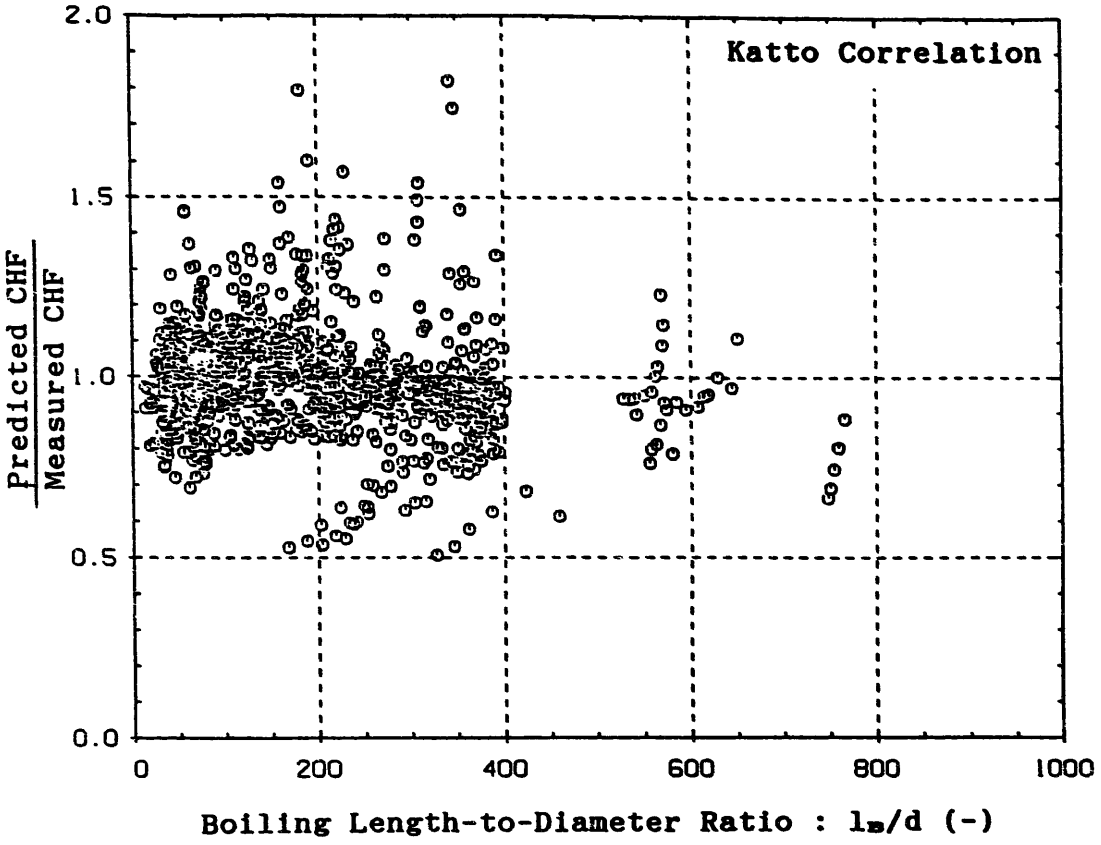

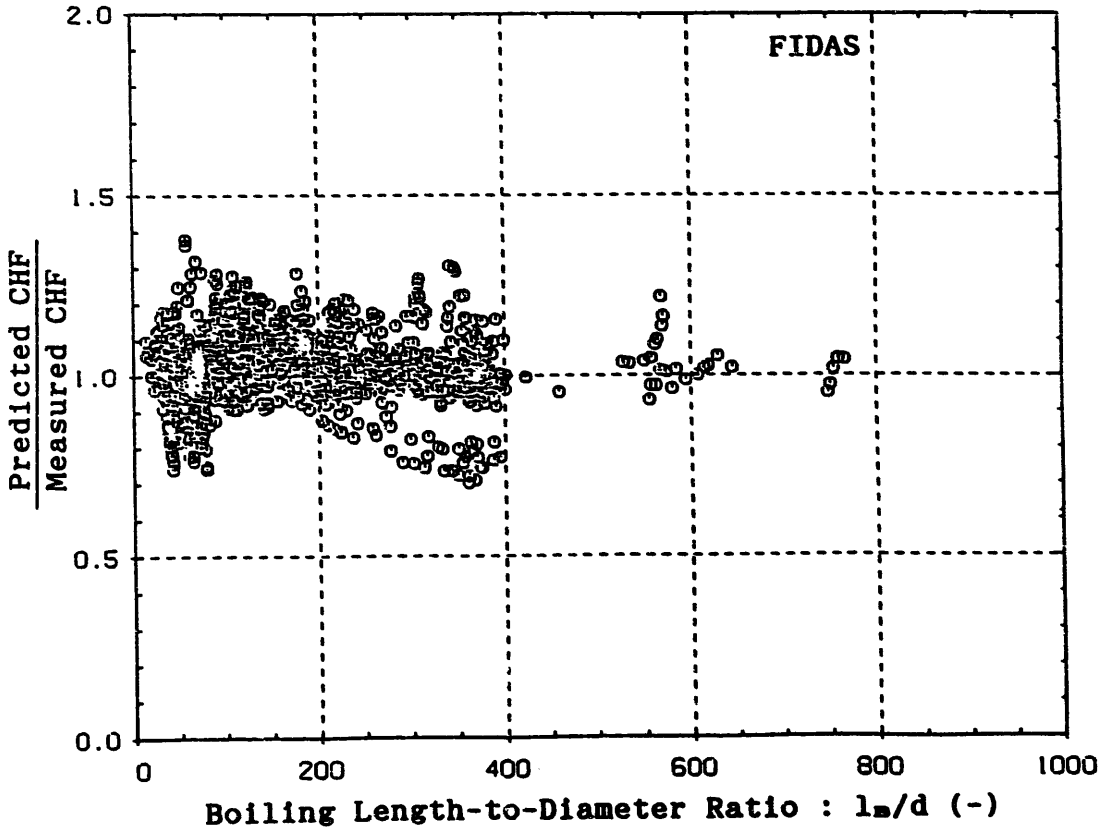

Fig.22 Examination of CHF Prediction Capability comparing with Katto's Correlation (#6: Dependence of CHF on Boiling Length)

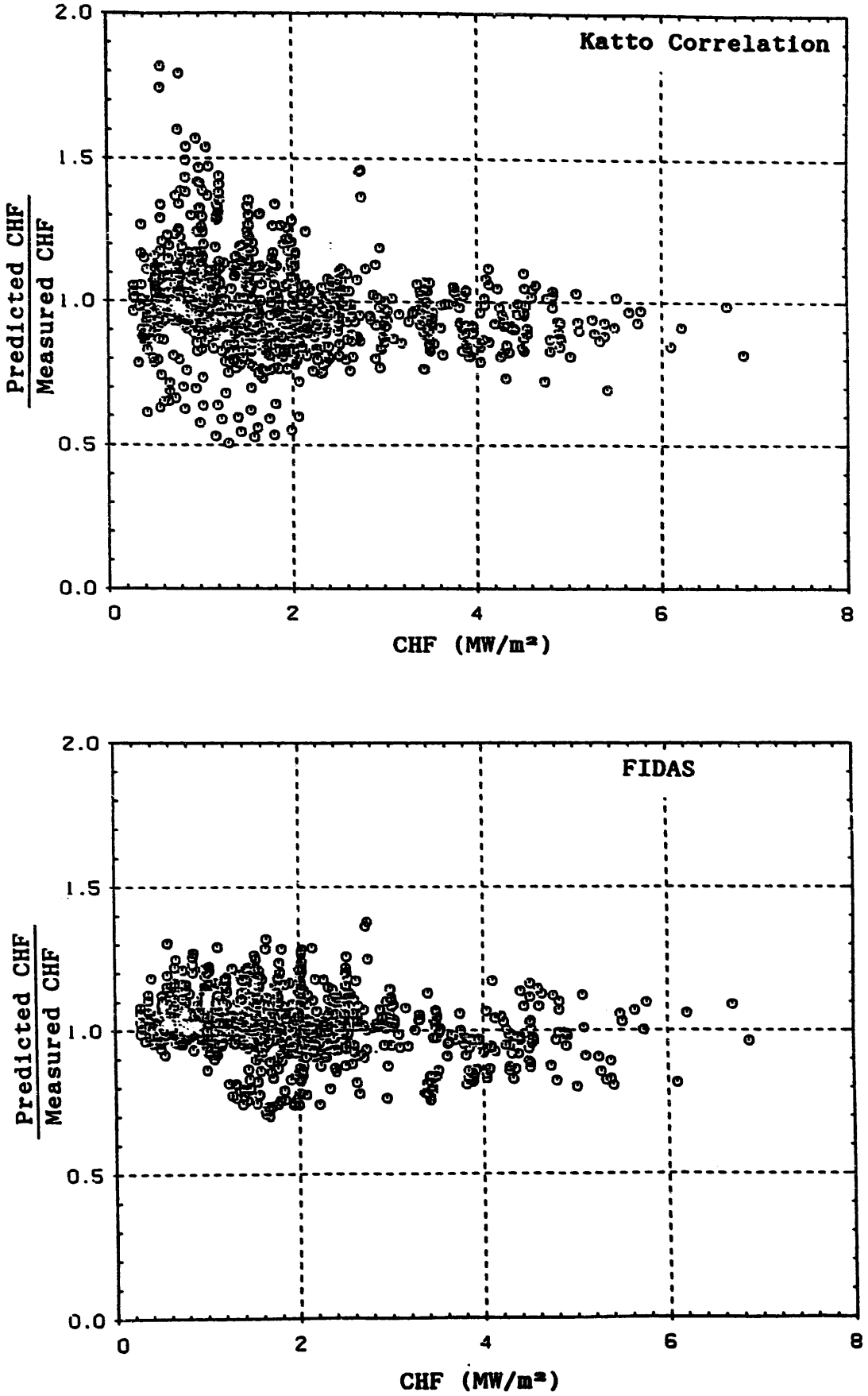

Fig.23 Examination of CHF Prediction Capability comparing with Katto's Correlation (#7: Prediction Accuracy vs. CHF)

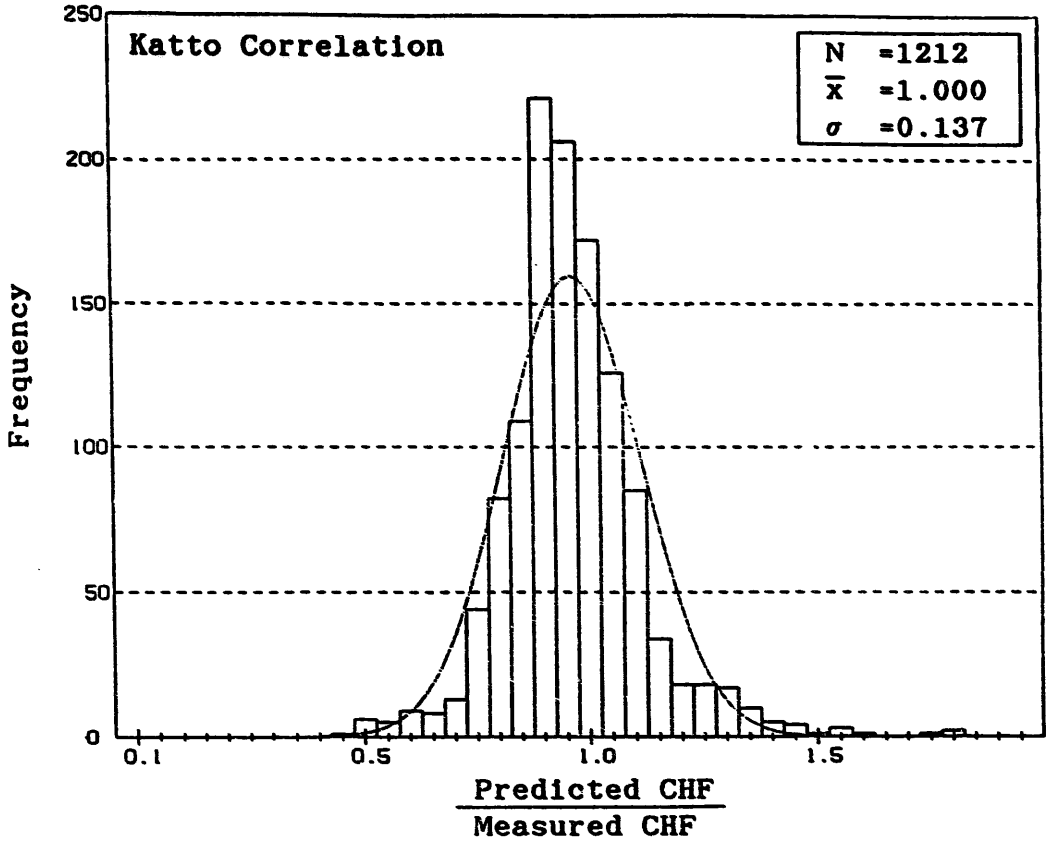

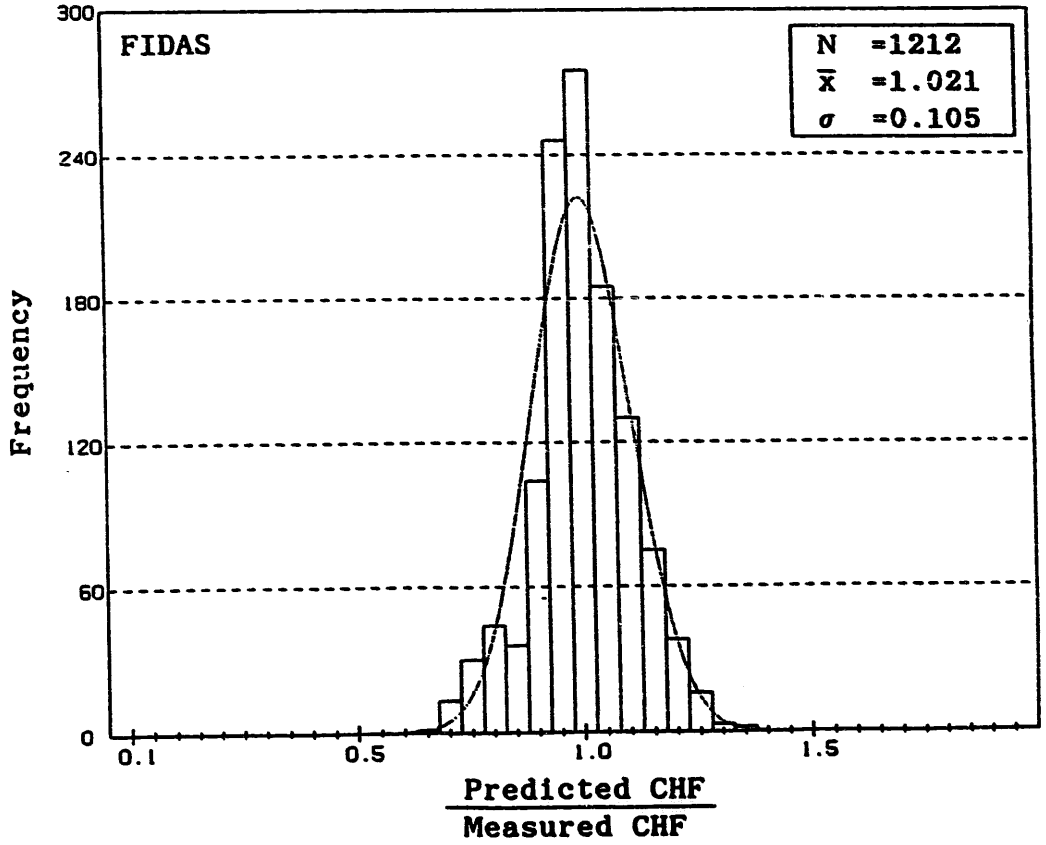

Fig.24 Histogram of (Predicted CHF)/(Measured CHF) comparing with Katto's Correlation